Influence of Physical Variability of Highly Weathered Sedimentary Rock on Nitrate in Area 3 of the ENIGMA Field Research Site at Y-12

A Thesis Presented for the
Master of Science
Degree
The University of Tennessee, Knoxville

Erin Kelly

December 2021

This thesis is dedicated to my fiancé, Ian Paterson, for his endless support and encouragement during my time as a master's student. He helped me with many computer-related questions and wouldn't let me give up.

Acknowledgments

I would like to thank my advisor, Dr. Terry Hazen, and my committee members, Dr. Annette Engel and Dr. Larry McKay, for their guidance and support throughout my master's project. Also, I'm extremely grateful for Andrew Putt for developing the RockWorks models and many of the figures. Katie Walker, Dominique Joyner, and Isis Fukai in Dr. Hazen's lab group helped me with field work, sampling, and poster collaboration and I'm thankful for their support. In addition, I greatly appreciate the hard work and dedication that the field crew with Fugro expressed while completing the cone penetrometer testing. That field work was made possible by the effort and support of our Radiological Control Technicians, Mike Cooke, Joel Miller, and Alex Patton, as well as our CPT rig operators, Bobby Brandt and Tyrone Sanders. We would like to thank Astrid Terry at Lawrence Berkeley National Laboratory and Ryan Post and Firas Mishu at M&W Drilling and Dennis Stauffer at Fugro for their support and effort in securing contracts to complete this work. I would also like to thank Miguel Rodriguez Jr. and Kenneth Lowe at Oak Ridge National Lab for assisting me in the field and lab. I want to thank Scott Painter, Scott Brooks, Betsy Romero, Walt McNab, Saul Montoya, Richard Winston, and David Parkhurst for answering my multitude of questions about MODFLOW and ModelMuse. This thesis would not have been possible without them. Also, I'm extremely grateful for my family and friends for their continued support throughout this process and believing in me. I'd also like to acknowledge COVID-19, which created an interesting experience the second half of my master's project. Finally, I'd like to thank my collaborators with ENIGMA at Lawrence Berkeley National Lab, University of Oklahoma, University of Georgia, University of Washington, and Montana State University. This material by the ENIGMA, Ecosystems and Networks Integrated with Genes and Molecular Assemblies (http://enigma.lbl.gov), a Science Focus Area Program at Lawrence Berkeley National Laboratory, is based upon work supported by the U.S. Department of Energy, Office of Science, Office of Biological & Environmental Research under contract number DE-AC02-05CH11231. Oak Ridge National Laboratory is managed by UTBattelle, LLC, for the U.S. Department of Energy under contract DE-AC05-00OR22725.

Abstract

Uranium processing and waste storage in unlined waste ponds leached contaminants into the groundwater at Y-12, Oak Ridge, Tennessee, from the 1950s to 1980s. Groundwater wells near the S-3 ponds have had the highest nitrate concentrations of groundwater anywhere in the world (>10,000 mg/L). For reference, the maximum contaminant level for nitrate in drinking water set by the U.S. Environmental Protection Agency is 10 mg/L. Since 2012, the ENIGMA (Ecosystems and Networks Integrated with Genes and Molecular Assemblies) group has been characterizing, monitoring, and conducting field experiments to understand the interactions between contaminants, microbes, and the subsurface. The goals of this project are to measure the variability of physical and hydrogeological properties in the weathered sedimentary rock (i.e., saprolite), (ii) determine how physical properties control contaminant distribution, and (iii) assess nitrate and geochemical correlations, which could provide insight into nitrate transformation processes. Physical characteristics of the shallow subsurface materials were evaluated using cone penetrometer testing (CPT) in 131 locations. Profiles of material type and hydraulic conductivity were generated from the CPT data. Colloidal borescope measurements from ENIGMA wells confirmed groundwater flow is to the south, away from the S3 ponds (now a parking lot), to Bear Creek. Slug tests were performed in six wells to calculate hydraulic conductivity, which ranged from 0.06 (at well FW115-32) to 3.5 m/day (at well FW127). Nitrate concentrations and other geochemical parameters were measured from ten wells. Hydraulic conductivity values estimated by the CPT corresponded to hydraulic conductivity values measured by slug tests in nearby wells. The study concludes that there is lateral connectivity amongst neighboring soil types and that the distribution of soil types across Area 3 is highly variable. Saprolite above the interface with intact rock generally has higher hydraulic conductivity values compared to the shallower saprolite and nitrate concentrations do not appear to have a relationship with hydraulic conductivity. Regions of low nitrate concentrations may be due to flushing by flow through fractures and high concentrations of nitrate may be attributed to low hydraulic conductivity and groundwater being in a state of sulfate reduction or methanogenesis.

Table of Contents

List of Tables

List of Figures

Chapter 1 Introduction

1.1 Background

The Oak Ridge Reservation (ORR) in Oak Ridge, Tennessee, has two main hydrologic units, the Knox Aquifer (primarily carbonates) and the ORR aquitards (primarily shale or interbedded shale and carbonate rock)[1]. The site geology controls the topography, with units that are more resistant to weathering forming ridges (i.e., sandstone or carbonates containing high content of clastic materials) and units that are less resistant to weathering (i.e., carbonates or weakly cemented shale) forming the valleys. Bedding of the units dip steeply (20-40 degrees) to the southeast. Bedrock is overlain by a layer of fine-grained, highly weathered or decomposed rock, typically varying in thickness from 2-10 meters. If the weathered material retains significant bedding and fractures from the parent bedrock, as is typical for the shale units, it is referred to as saprolite. If the weathered material has a massive fabric, with no visible sedimentary layering, it is referred to as residuum. The saprolite units imply very little loss of rock volume during weathering, whereas the residuum developed on carbonates typically represents very large volume losses (up to 90-95% for a parent carbonate rock with 5-10% detrital material). Soils are immature and very thin, with the A and B horizons often less than 60 cm in thickness. In some areas, fill materials from road or building construction, are present in the upper 1-2 meters.

Groundwater flow and hydraulic conductivity in the subsurface are strongly influenced by the properties of the bedrock, soil, saprolite, and residuum, as well as the steep topography[2, 3]. This leads to shallow infiltration and rapid downslope flow and discharge into local streams. Rapid transport can occur in coarse layers of fill material or along naturally occurring layers of chert fragments, which are common in some of the residuum materials derived from carbonate bedrock. But, fractures and bedding planes, as well as by dissolution along flow pathways in the carbonate rocks[4], control the underlying bedrock hydraulic conductivity. Hydraulic conductivity of the shale bedrock is generally lower than that of the overlying weathered materials, but is highly variable in the carbonate bedrock[1]. The spacing, interconnectivity, and aperture of these fractures and bedding planes vary in the saprolite and residuum. High hydraulic conductivity zones often occur in the upper meter, due to root holes and other soil features, as well as in the saprolite or residuum immediately above the transition to bedrock. In some cases, high hydraulic conductivity occurs at the intersection of bedding planes and cross-cutting tectonic fractures, especially in the saprolite, which results in preferential transport parallel to the strike of bedding[5]. Hydraulic conductivity of the fine-grained "matrix" of the highly weathered materials can be much lower than the bulk hydraulic conductivity. Moreover, variability in hydraulic conductivity with depth can also be due, in part, to the occurrence of a "hardpan" layer below the root zone where the fractures and root holes are largely infilled with translocated pedogenic clays from the overlying soil zones[2].

Many experimental investigations have been carried out to understand contaminant transport in the weathered materials, mainly at uncontaminated ORR sites. Contaminant transport reflects the hydraulic conductivity of different materials. In the highly weathered zone, fractures, root holes, and bedding planes strongly influence advective transport, but relatively immobile pore-water in the fine pore structure results in matrix diffusion[4]. Matrix diffusion causes flow retardation, differential transport of non-reactive solutes and colloidal particles[4, 6], and storage of contaminants[3, 5, 7], with diffusive exchange between pore water in the fractures and in the matrix being affected by ionic strength and cation exchange[7]. It can also result in the release of solutes over long periods of time after a contaminant source is removed. Sorption is also an important factor, for the transport of some contaminants, because of the potential for attachment of contaminants to both the walls of the fractures or macropores and attachment to the very large surface area available in the fine-grained matrix. To clarify the differences in flow rates, one experimental field study at an uncontaminated ORR site[6] released dissolved tracers and colloidal tracers in a well completed just above the saprolite-bedrock. Appearance of tracers was monitored in wells located from 2 to 35 m downslope of the injection well. The dissolved tracers (fluorescent dyes) took up to two years to travel to the furthest downslope well, whereas the colloidal tracer (fluorescent microspheres and bacteria) was transported the same distance in a matter of hours or days. Matrix diffusion was responsible for the large difference in transport rates for solutes and colloidal particles[6].

Despite these past research efforts, there is still relatively little information on how geological material properties, specifically of the saprolite, control the distribution of contaminants at contaminated sites at ORR. Consequently, the goals of this study were to (i) measure the variability of physical and hydrogeological properties in the weathered materials (i.e., saprolite) at a contaminated site, specifically with nitrate, (ii) determine how physical properties control contaminant distribution, and (iii) assess nitrate and geochemical correlations, which could provide insight into nitrate transformation processes.

1.2 Study Site

Since 2012, the ENIGMA (Ecosystems and Networks Integrated with Genes and Molecular Assemblies) group at the Department of Energy's Biological and Environmental Research, Oak Ridge National Laboratory (ORNL) field research site (DOE BER FRC) has been characterizing, monitoring, and conducting field experiments to understand how contaminants move in the shallow subsurface and to elucidate the fundamental mechanisms of microbes cleaning up environmental pollution at Area 3 in Y-12 in the Bear Creek Valley[8] (Figure 1). This work has involved several field studies, including pump tests, hydrological modeling, characterization of sediment and groundwater, and characterization of amendments of emulsified vegetable oil, ethanol, bromide, and nitrate. Over the past 40 years, hundreds of wells have been established and characterized as a part of a variety of operations[9].

As part of processing uranium waste at Y-12, four unlined ponds, about 5.2 m deep and 122 m long on each side, were constructed in 1951. Each waste pond had a total holding capacity of 9.5 million liters. Initially, the main waste was 30% uranium nitrate, received at a rate of 10 million liters per year until 1983. The S-3 waste ponds also held waste from other related sites, such as the Savannah River site, Oak Ridge, Idaho National Engineering Lab, and East Tennessee Technology Park. In 1962, the total nitrate content of the waste ponds was 2,263,000 kg; in 1978, the highest nitrate concentration found in the waste ponds was 73,840 mg/l[10]. In 1988, waste was treated *in situ* through neutralization and biodenitrification[10], the ponds were capped, and then covered by asphalt to form a parking lot. There is no record of the total nitrate concentration of the ponds before they were capped, but the concentration can be estimated by using estimates of the total mass of nitrate added and the total volume of the ponds.

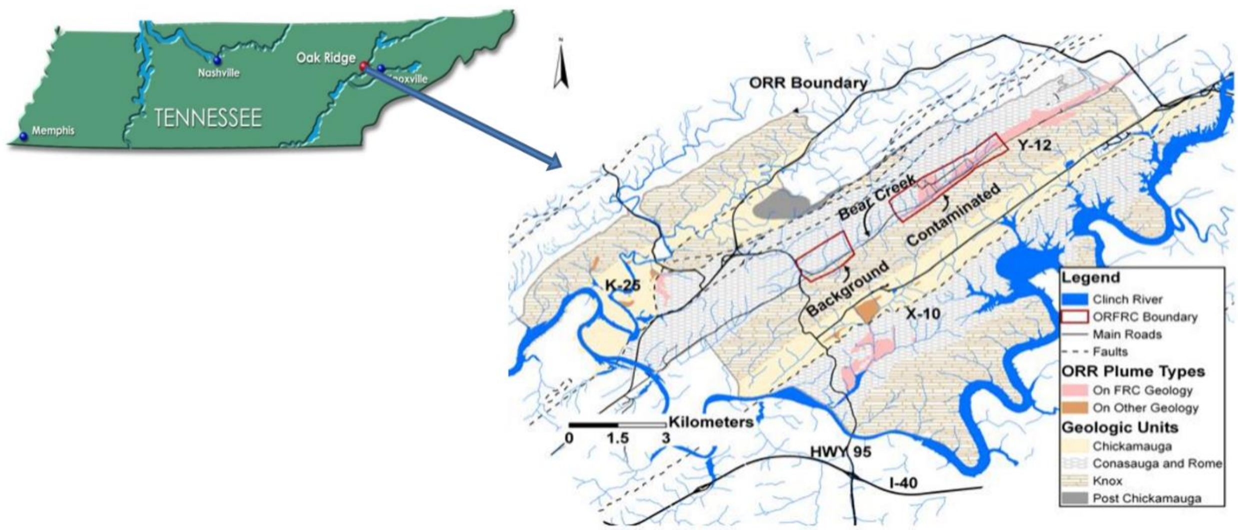

Figure 1: Overview of the geology and contamination plumes that make up the Oak Ridge Reservation (ORR), which is located within Bear Creek Valley in eastern Tennessee.

Area 3 is located west of the S-3 waste ponds (Figure 2). Area 3 is underlain by the Knox Aquifer composed of the Copper Ridge Dolomite of the Knox Group and underlying Maynardville Limestone and Nolichucky Shale of the Conasauga Group. Three main fracture sets have been identified in these rock units, including parallel to bedding, perpendicular to bedding, and vertical-parallel to dip. Rocks dip 45 degrees to the southeast and have a strike of N55E[11] (Figure 3). The depth to groundwater is approximately 3.5 meters from the surface and the hydraulic gradient is low and typically towards Bear Creek, to the south of Area 3[9]. About one meter of reworked fill overlies the saprolite[12]. The saprolite in the southern portion of Area 3 is about 15.6 meters thick, but only about 2 to 3 meters thick in the northern portion.

Nitrate and uranium contamination is detected at higher concentrations in the shallow saprolite wells, intermediate-depth saprolite wells, and deep bedrock wells, as well as solid phases (i.e., soil), of Area 3 relative to Areas 1 and 2 (Figure 2). Nitrate concentrations in Area 3 groundwater are approximately 9,000 mg/l and uranium is as high as 60 mg/l[10]. The pH of groundwater in Area 3 is also typically around 4, which suggests that it is acidic enough to dissolve carbonate bedrock and saprolite[9]. Contaminant transport in the saprolite underlying Area 3 is expected to be controlled mainly by advective transport along fractures and bedding planes, combined with diffusion into relatively immobile pore water in the fine-grained matrix (i.e., matrix diffusion). The deep saprolite zone is likely a preferential pathway for contaminant transport from the S-3 waste ponds[13]. Previous studies from wells that were spaced far apart from each other indicated that the hydraulic conductivity of the shallow saprolite is less than 0.26 m/day, while the groundwater flux of the deeper saprolite in the southern portion of the site is around 0.5 m/day[9].

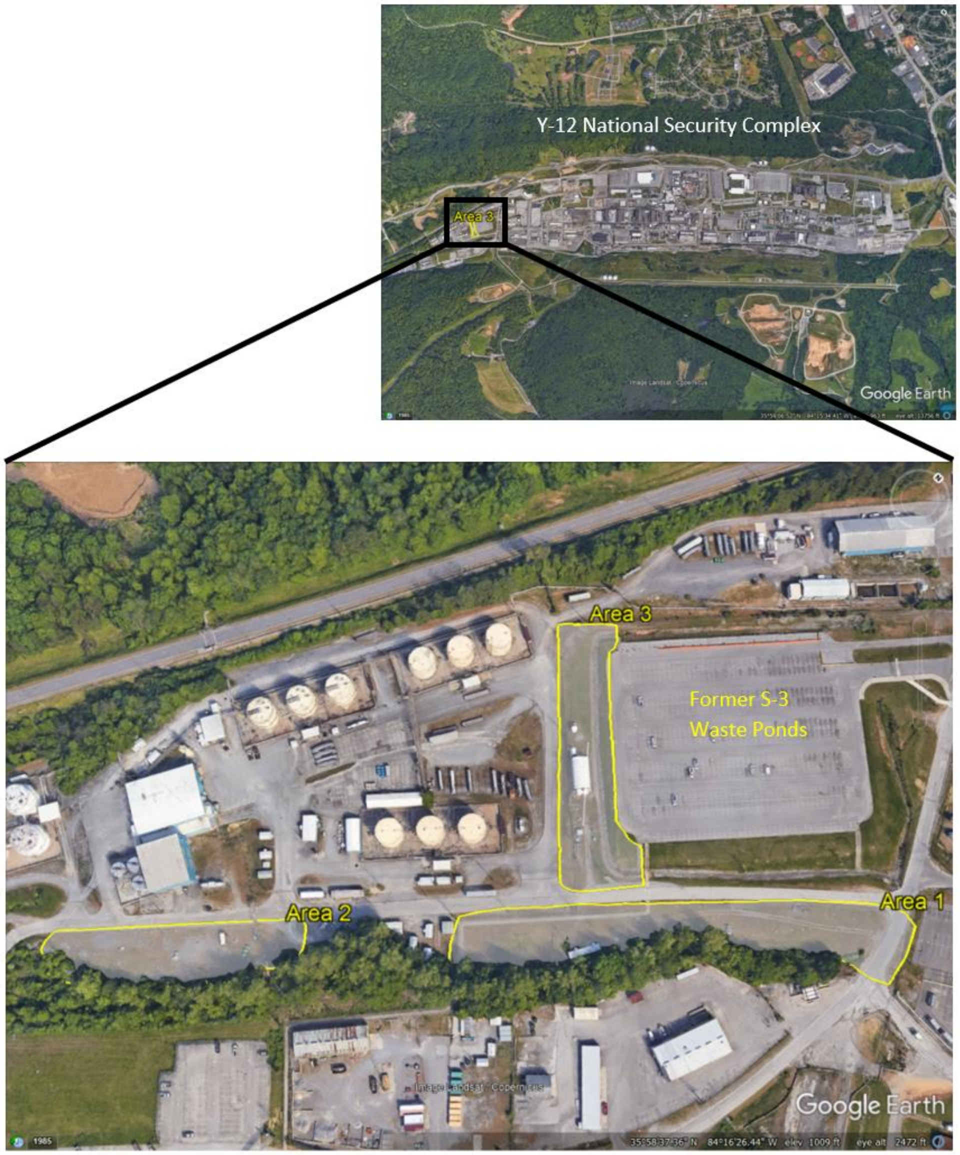

Figure 2: The location of Area 3 relative to Y-12 National Security Complex, Areas 1 and 2, and the former S-3 waste ponds, which are now a parking lot, Oak Ridge, TN.

Top image: 35° 59' 06.92"N, 84° 15' 34.41"W, eye alt 13,756 feet; bottom image: 35° 58' 37.36"N, 84° 16' 26.44"W, eye alt 2472 feet). Images obtained from Google Earth V 7.1, Image Landsat/Copernicus (April 3, 2021), http://www.earth.google.com [last accessed August 9, 2021].

Figure 3: A road cut near Oak Ridge National Lab and Y-12 National Security Complex, showing the 45° dip of the shales.

Chapter 2 Goals, Objectives, and Hypotheses

2.1 Goals

The main goals of this study are to (i) measure the variability of physical and hydrogeological properties in the weathered materials (i.e., saprolite) at Area 3, (ii) determine how the physical and hydrogeological properties control the distribution of nitrate contamination from the S-3 pond, and (iii) assess nitrate and geochemical correlations, which could provide insight into nitrate transformation processes.

2.2 Objectives

1. Use cone penetrometer testing (CPT) to get a 3-D view of the geological materials in the shallow subsurface across Area 3.
2. Determine the lateral and vertical distribution of hydraulic properties in the weathered subsurface materials of Area 3 using CPT, slug tests, colloidal borescope, and water level measurements.
3. Measure nitrate and geochemical parameters from groundwater in the saprolite in Area 3 and evaluate the composition relative to lithologic and hydraulic properties.
4. Assess the spatial concentrations of nitrate and other geochemical parameters to address if or to what extent nitrate transformations are occurring at Area 3.

2.3 Hypotheses

1. Material type in the highly weathered materials overlying bedrock in Area 3 will show lateral connectivity along the direction of the dip of bedding of the parent bedrock (i.e., to the southeast).
2. High hydraulic conductivity values estimated from CPT profiles will correspond with zones of higher hydraulic conductivity measured in nearby wells using slug tests and vice versa.
3. The deep saprolite will have higher hydraulic conductivity values than the shallow saprolite.

4. Nitrate concentrations are expected to be higher in zones of low hydraulic conductivity, as estimated by CPT data and measured using slug tests in wells, because of retention of nitrate in relatively immobile pore water in these zones.

Chapter 3 Methodology

3.1 Cone Penetrometer Testing

Cone penetrometer testing (CPT) was completed to obtain a detailed 3-dimensional view of the lithology layers that make up the shallow subsurface of Area 3. Figure 4 shows the cone penetrometer sensor, truck, and an example lithology type profile that's produced. Figure 5 shows a map of all the CPT pushes that were done. Field work for CPT consisted of 16 days of pushes, from 2020-10-12 to 2020-10-27. The cone sensor was calibrated before every push and advanced until the cone hit refusal. The CPT data for each borehole included sleeve friction, cone resistance, pore pressure, friction ratio, and soil behavior type[14]. Holes were grouted after completion with a bentonite clay slurry. As the probe was pushed through the subsurface materials, load cells embedded in the sleeve of the cone, 10 cm behind the tip, measured the sleeve friction, which is the friction of the horizon being penetrated. The sleeve friction and cone resistance were measured in tons per square foot (TSF). Pore pressure was measured in the piezocell in pounds per square inch (psi), either while advancing or stationary[15]; higher pore pressure readings resulted when the cone penetrated dense lithology layers. The friction ratio is the ratio of sleeve friction divided by the cone resistance and was recorded in percent. High ratios corresponded to clayey lithologies and low ratios corresponded to sandy lithologies[14]. The CPT profiles were based on 12 soil behavior types[16], proposed by Robertson et al. (1986)[17], but later simplified to nine types by Robertson et al. (1990)[18].

3.2 Lithology Models

The Rockware® (Golden, CO) Rockworks2020 program (version 2021.3.31) was used with the CPT data to create a cross-sectional model of the stratigraphy. Lithology types, cone pressures, and geochemical data were mapped to determine the extent of shallow subsurface lithology layers. The lithology relating to soil types was saved as a data object in Rockworks called 'point-data'[19]. The provided profile of Area 3 was generated by interpreting the point-data across Area 3. A subsite was generated for all of Area 3 using a 5% distance barrier in the X, Y, and Z profiles according to the CPT borehole locations and depths. The CPT data existed in the X and Y directions, whereby a polygon filter was applied to set the Area 3 boundary and exclude

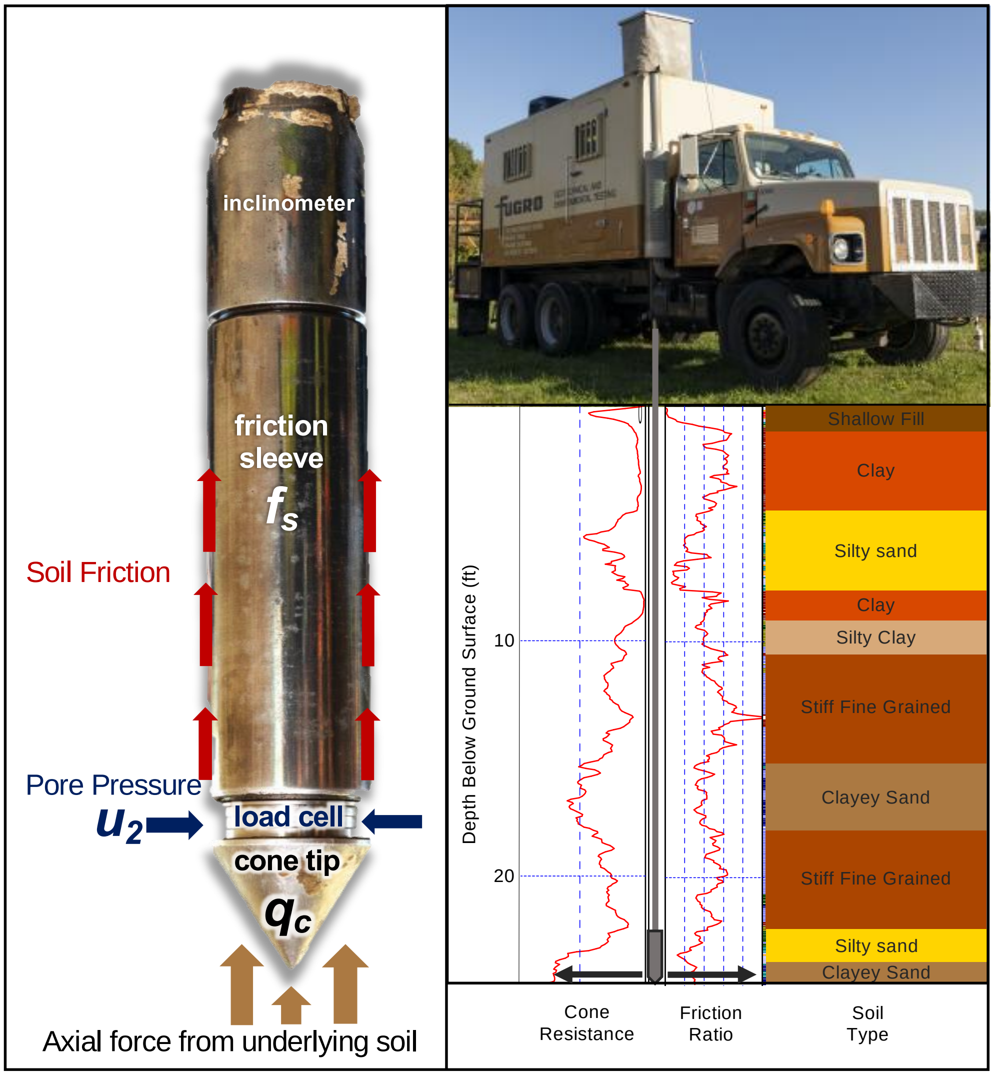

Figure 4: The cone sensor, CPT truck, and an example lithology type profile produced as the cone advances. The cone sensor measures the pore pressure, soil friction, and cone resistance to identify the lithology types that make up the shallow subsurface[20].

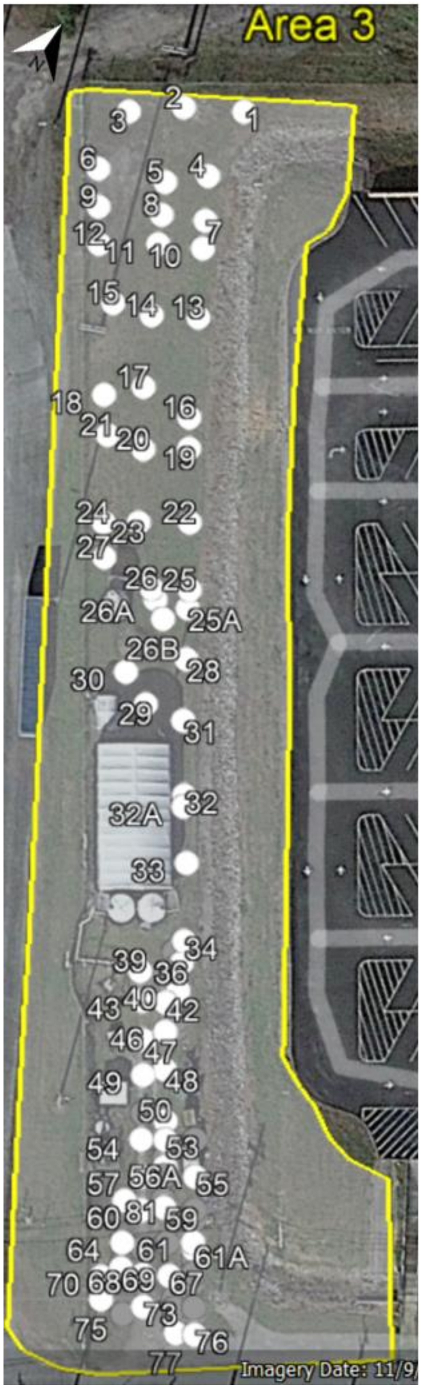

Figure 5: Map view of CPT pushes (numbered dots) in Area 3, Oak Ridge, TN.

Image location, 35° 58’ 39.08”N, 84° 16’ 25.15”W, eye alt 635 feet. Image obtained from Google Earth, Image Landsat/Copernicus, http://earth.google.com [last accessed October 23, 2021].

the area under the storage building in Area 3. In the Z profile, CPT pushes that reached early refusal, attributed to buried debris as opposed to bedrock, were excluded from analysis because their profiles were limited and inaccurately shaped the base elevation profile. Base elevations were used to create the model subface. The three-dimensional volume was broken into cubes called voxels. In the X and Y directions, the voxels were 0.5 m by 0.5 m; in the Z direction, the voxel was 0.2 m. Because the CPT data were categories, lithology and soil types were solved for using a horizontal lithoblending model, which was a simple solution built from expanding cylinders emanating from each CPT core. Appendix B contains the methods and results for the exploratory nitrate models that were completed using the lithology models.

3.3 Colloidal Borescope

Colloidal borescope measurements were taken in Area 3 at wells FW127 and FW128 to produce a vector field of the estimated groundwater flow pathways on 2021-03-12. These wells were used because they were a large enough diameter to fit the colloidal borescope, but not so large that packers would be needed to section off the well. The diameter of some of the other shallow wells was not large enough to fit the colloidal borescope, so those flow vectors and flow zone depths could not be measured. Figure 6 is a map showing where wells FW127 and FW128 are, as well as the other wells analyzed in this study, and Table 1 summarizes the analyses and tests completed on each well. The colloidal borescope used a high-resolution motion picture camera and compass to track the direction and speed of colloids in the groundwater. The new flow vectors were compared to the old vector measurement in well FW106 from the ENIGMA 27 well survey[21].

3.4 Water Levels and Slug Tests

Water level measurements were taken using a Solinst Model 102 water level meter (marked every 1/100 ft and conductivity sensitivity = 40 µS/cm) nearly every day that CPT investigations were in progress, and before groundwater sampling. Table 2 contains well construction data for all the wells referenced in this study and Table 3 contains initial pumping

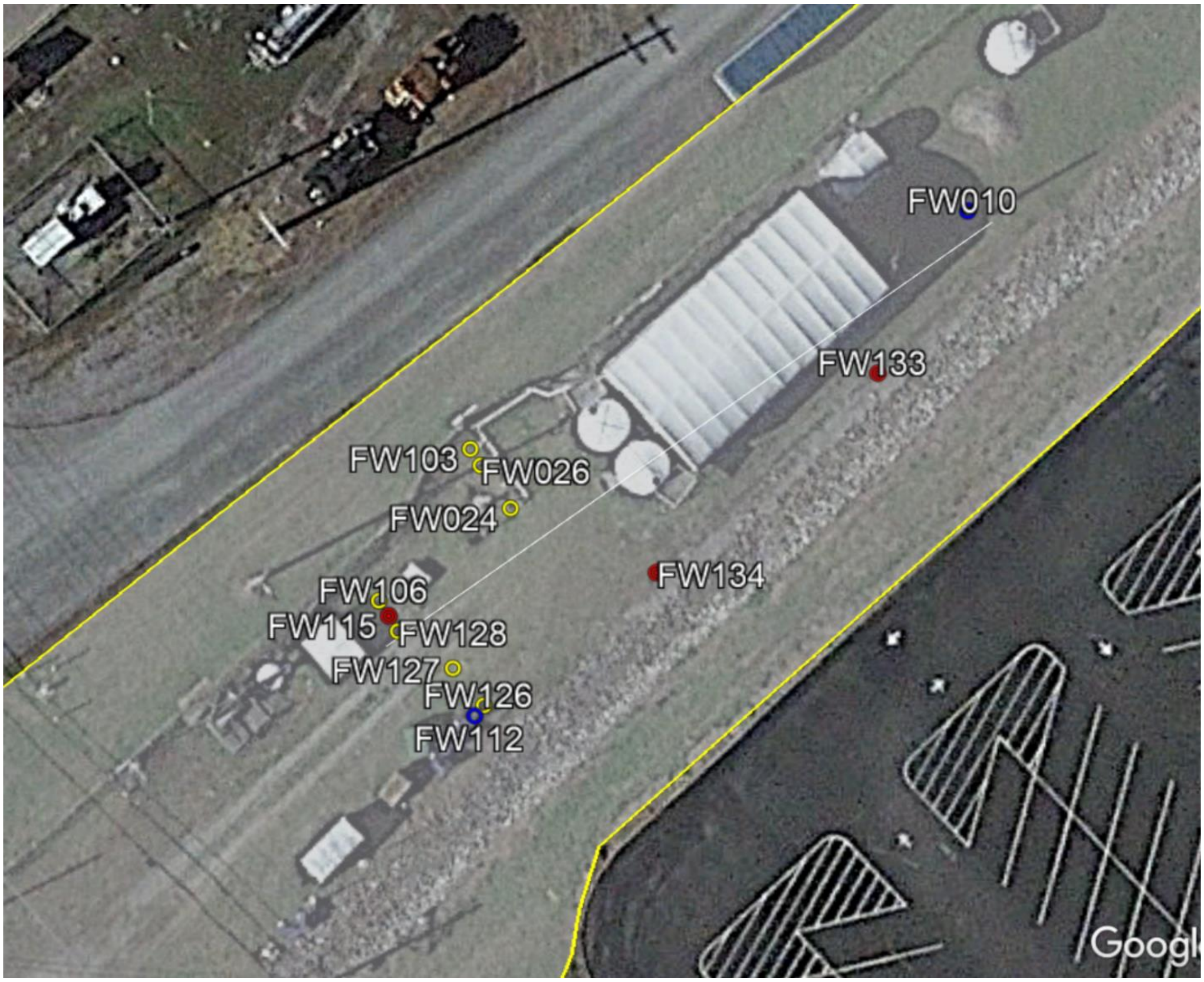

Figure 6: Map of the 12 Area 3 wells referenced in this study.

Image location, 35° 58' 38.61"N, 84° 16' 24.70"W, eye alt 251 feet. Image obtained from Google Earth, Image Landsat/Copernicus, http://earth.google.com [last accessed October 23, 2021].

Table 1: Summary of field analyses done and data types resulting from each groundwater well used in this study (section numbers refer to where methods for each types of analyses can be found in the thesis).

Well	Nearby CPT Push Number (Section 3.1)	Collodial Borescope (Section 3.3)	Slug Test (Section 3.4)	Water Level Datalogger (Section 3.4)	Geochemical Data (Section 3.5)
FW010	CPT-29	No	Yes	No	Yes
FW024	CPT-39	No	No	Yes	Yes
FW026	CPT-39	No	No	No	Yes
FW103	CPT-39	No	Yes	Yes	Yes
FW106	CPT-49	Yes, previous study[21]	No	No	Yes
FW112	CPT-48	No	No	Yes	No
FW115-32	CPT-49	No	Yes	No	No
FW126	CPT-48	No	No	No	Yes
FW127	CPT-46A	Yes	Yes	No	Yes
FW128	CPT-49	Yes	Yes	No	Yes
FW133-1	CPT-32	No	Yes	No	Yes
FW134-2	CPT-34	No	Yes	No	Yes

Table 2: Area 3 well casing elevation, screened interval, and casing depth.

Well	Top of Casing Elevation (m AMSL)[1]	Screen Start Depth (m BGS)[2]	Screen End Depth (m BGS)	Well Casing Depth (m BGS)
FW010	308.9	5.71	6.58	6.58
FW024	308.1	11.81	13.74	13.97
FW026	307.9	11.74	13.67	13.90
FW103	307.8	11.78	13.71	13.94
FW106	307.4	10.74	13.72	13.79
FW126	308.5	12.25	15.12	15.24
FW127	308.4	12.18	15.04	15.24
FW128	308.1	12.41	15.11	15.28
FW133-1	308.8	6.04	7.13	7.21
FW134-2	308.6	6.07	7.54	10.96
FW112	308.5	8.55	9.96	10.04
FW115-32	307.7	8.70	9.58	9.63

[1]AMSL = above mean sea level
[2]BGS = below ground surface

Table 3: The depth to water measurements, pumping rate, and volume of water pumped on the first day of field work.

Well	Depth to Water (m)	Pumping Rate	Volume Pumped
FW010	3.01	170 mL/min	8 L
FW024	3.74	110 mL/min	8 L
FW026	3.55	150 mL/min	8 L
FW103	3.55	150 mL/min	8 L
FW106	3.62	130 mL/min	8 L
FW126	4.16	170 mL/min	8 L
FW127	4.04	170 mL/min	8 L
FW128	3.12	170 mL/min	8 L
FW133-1	3.45	170 mL/min	8 L
FW134-2	3.86	170 mL/min	8 L
FW112	4.05	N/A	N/A
FW115-32	3.93	N/A	N/A

conditions for the wells that were sampled and had aquifer tests performed. During pump and slug tests, and colloidal borescope measurements, water level was continuously monitored using an Aqua TROLL® 500 and Level TROLL® 400 (both from In-Situ Inc.). The pressure and temperature sensors have an accuracy of ±0.05%, while the temperature sensor has a separate accuracy of ±0.1°C, pH has ±0.1 pH unit or better, barometric pressure has ±1.0 mbars, ORP has ±5 mV, conductivity has ±0.5%, dissolved oxygen has ±0.1 mg/L and ±2% of reading, and turbidity has ±2% of reading or ±0.5 NTU. Slug tests, which measured hydraulic conductivity values in selected wells, were done by abruptly raising or lowering the hydraulic head in a well and monitoring the rate of recovery to pre-test levels. In this study, rising-head slug tests were performed on wells FW010, FW103, FW115-32, FW127, FW134-2, and FW128 on 2020-11-09 and 2020-11-10. A rising head slug test was also performed on FW133-1, but it recharged so quickly that the hydraulic conductivity had to be estimated. These wells were chosen because of their distribution across the site. Depths of the screened portions of the wells, where the hydraulic conductivity values were measured, varied from 5.71 to 15.11 m below surface. An Excel spreadsheet was used to run the Hvorslev analysis to calculate the hydraulic conductivity values[22]. Table 4 shows the inputs to the excel spreadsheet and the slug dimensions for each well.

3.5 Geochemical Analyses

Groundwater sampling was carried out at 10 wells across the southern and middle portions of Area 3 from 2020-09-30 to 2020-10-01. The construction data for these wells can be found in Table 1. The screened intervals for the wells accessed shallow and deep flow paths[9], ranging from 5.71 to 7.54 meters deep or from 10.74 to 15.12 meters deep, respectively. Depth to water was measured before purging 8 L of water from each well, which was required for physicochemical parameters to stabilize, using a peristaltic pump, according to the EPA's sampling low flow guidelines[23]. Pumping rates ranged from approximately 110 ml/minute to 170 ml/minute (Table 2).

In-field measurements of temperature, redox potential, dissolved oxygen, specific conductivity, and pH were collected by using a calibrated multiparameter Aqua TROLL® 500

Table 4. Slug test inputs for excel Hvorslev analysis and slug dimensions

Well	Length Of Screen Interval – L (cm)	Well Inner Diameter – r (cm)	Borehole Radius – ‘r (cm)	Starting Depth To Water – H (cm)	Depth To Water After Slug is Removed – H_0 (cm)	H – H_0	Slug Dimensions (in)
FW010	86.87	1.91	1.35	296.57	324.92	-28.35	0.5 X 36
FW103	192.94	10.16	12.07	338.63	348.69	-10.06	3 X 36
FW115-32	88.09	1.53	4.13	348.39	395.63	-47.24	0.5 X 36
FW127	287.12	5.20	10.16	382.52	388.32	-5.79	1.5 X 36
FW128	270.36	5.20	9.21	288.34	302.06	-13.72	1.5 X 36
FW133-1	108.81	2.61	8.89	263.65	289.86	-26.21	1 X 36
FW134-2	142.34	3.45	4.45	386.18	412.09	-25.91	1 X 36

(In-Situ Inc.). Groundwater was filtered through a 0.2 µm pore diameter nylon syringe filter using a 25 mL sterile syringe into a sterile 50 mL polypropylene centrifuge tube[24]. Anions collected in the field were transported on ice (4°C) and analyzed within 24 hours of collection. Cations collected in the field were transported on ice (4°C) and were acidified with 10% 1M HCl. Anions and cations were measured by using ion chromatography (IC) with a Dionex ICS-5000+ (AS11-HC analytical column and CS12A analytical column, respectively), as described by King et al[25]. Due to low pH (<4) and high nitrate concentration, samples were diluted using Nanopure water (background conductivity 18.2 MΩ-cm). Alkalinity was measured from unacidified water by manual titration to pH 4.3 using 0.1 N sulfuric acid[26].

3.6 Statistical Analysis

Several different statistical analyses were completed in RStudio using the *tidyverse* and *ggplot2* packages[27, 28]. The Spearman correlation measured monotonic relationships among two continuous random variables when the data are not normally distributed. Concentrations were converted to mmol/L and the data were transformed to a log scale to account for differences in how data were collected, detection limits, ranges of values, and for non-normally distributed data. The correlation coefficient value ranged from -1 to 1 and the significance level was set at 0.05. Initial correlations for the linear regression model were determined using the Spearman test. A regression analysis was used to estimate relationships between nitrate concentrations and other geochemical conditions. Residuals were calculated to determine appropriateness in representation. The accepted significance level was set at 0.05 for the residuals and regression models. A paired t-test was used to calculate the significance between hydraulic conductivity values at the same depth estimated from the CPT push soil types and from slug test measurements at nearby wells. The accepted significance level was set at 0.05.

Chapter 4 Results

4.1 Subsurface Geology from Cone Penetrometer Testing

The CPT profiles revealed the geological materials in the shallow subsurface across Area 3. Figures 7, 8, and 9 are examples of CPT pushes, which were located near most of the wells that were sampled in this study, including CPT-7 and CPT-10, CPT-34 and CPT-36, and CPT-50 and CPT-52. Soil types interpreted from the CPT friction ratios were condensed to nine soil types based on hydraulic conductivities[16]. Similar hydraulic conductivities were grouped together to simplify the soil classifications into five general soil groups (Table 5). Group 1 had very low hydraulic conductivity, spanning 10^{-10} to 10^{-9} m/s. Group 2 was the largest group, as many of the soil units fell into this range of 10^{-10} to 10^{-7} m/s. Group 3 had a medium hydraulic conductivity, ranging from 10^{-8} to 10^{-3} m/s, and group 4 had a high hydraulic conductivity ranking, from 10^{-5} to 10^{-3} m/s. Group 5 had a very high hydraulic conductivity ranking that spanned from 10^{-3} to 1 m/s.

The paired CPT pushes revealed that physical properties of the shallow subsurface at Area 3 were highly variable over short distances and that there is lateral connectivity between soil types, suggesting that there may be several preferential flow paths. CPT pair CPT-7 and CPT-10 (Figure 7) had similar soil types. Their pore pressure and cone resistance profiles did not appear to match between the two pushes, but these correlations were not statistically tested. The same situation was observed with the soil behavior type profiles for CPT pair CPT-34 and CPT-36 (Figure 8), which indicated lateral connectivity between soil types within a couple meters of each other. This result supported hypothesis one. For example, the saprolite, at a depth of 12–14 m in the southern part of Area 3, could be a preferential pathway[11]. The saprolite and bedrock interface is near this depth, as well, which was when refusal was reached for the CPT drilling and prior well installation. Figure 10 shows sand, which had a high hydraulic conductivity range of 10^{-5} to 10^{-3} m/s, at the depth interval of 12-14 m to the right of CPT pairs 50 and 52. CPT-50 and CPT-52 appeared to have the most variation between their profiles, despite being only several meters apart from each other.

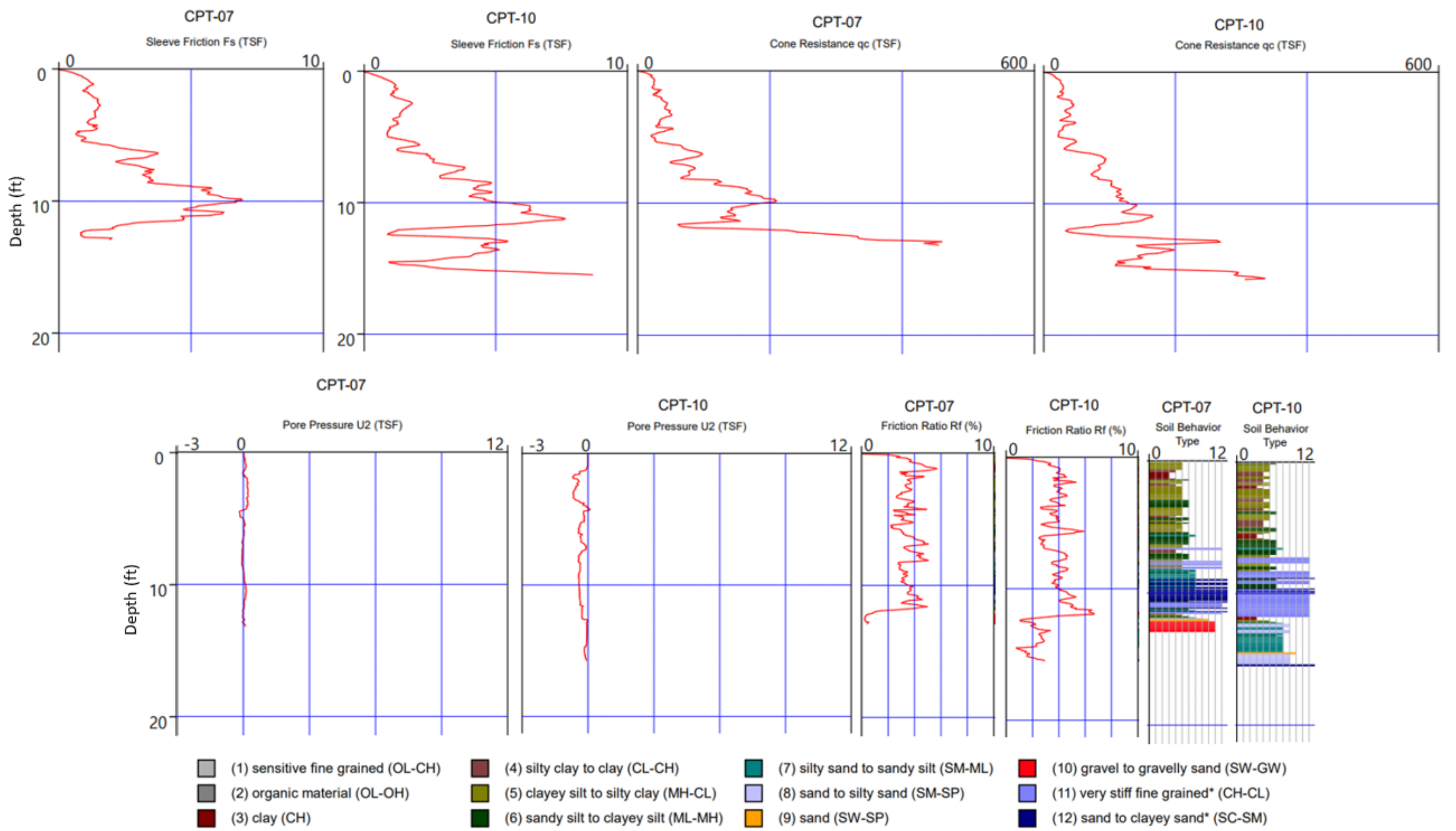

Figure 7: Side-by-side comparison of CPT-7 and CPT-10 profiles interpreted from the CPT software. The x-axis for the soil behavior type profiles are the 12 original soil behavior types[18].

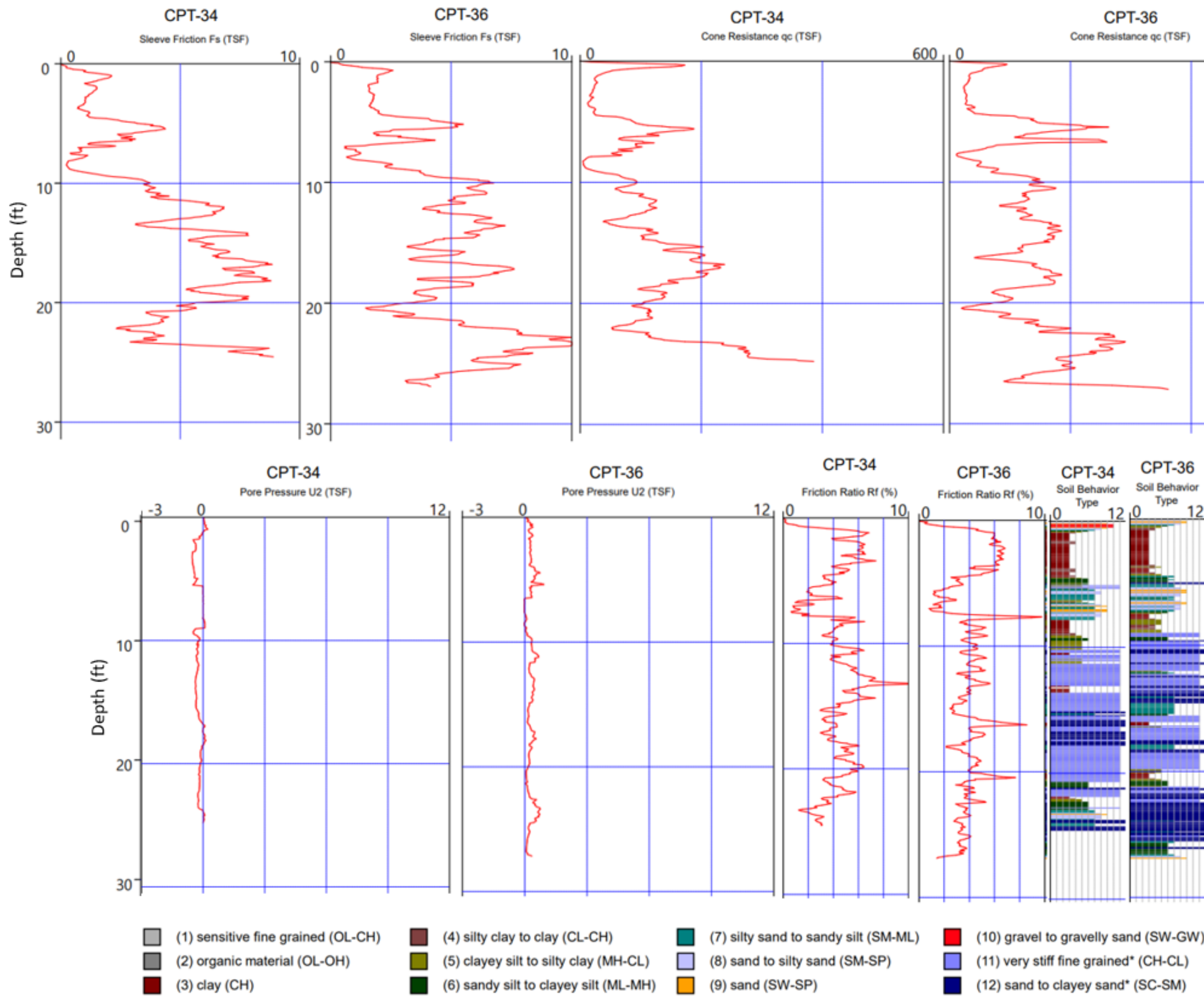

Figure 8: Side-by-side comparison of CPT-34 and CPT-36 profiles interpreted from the CPT software. The x-axis for the soil behavior type profiles are the 12 original soil behavior types[18].

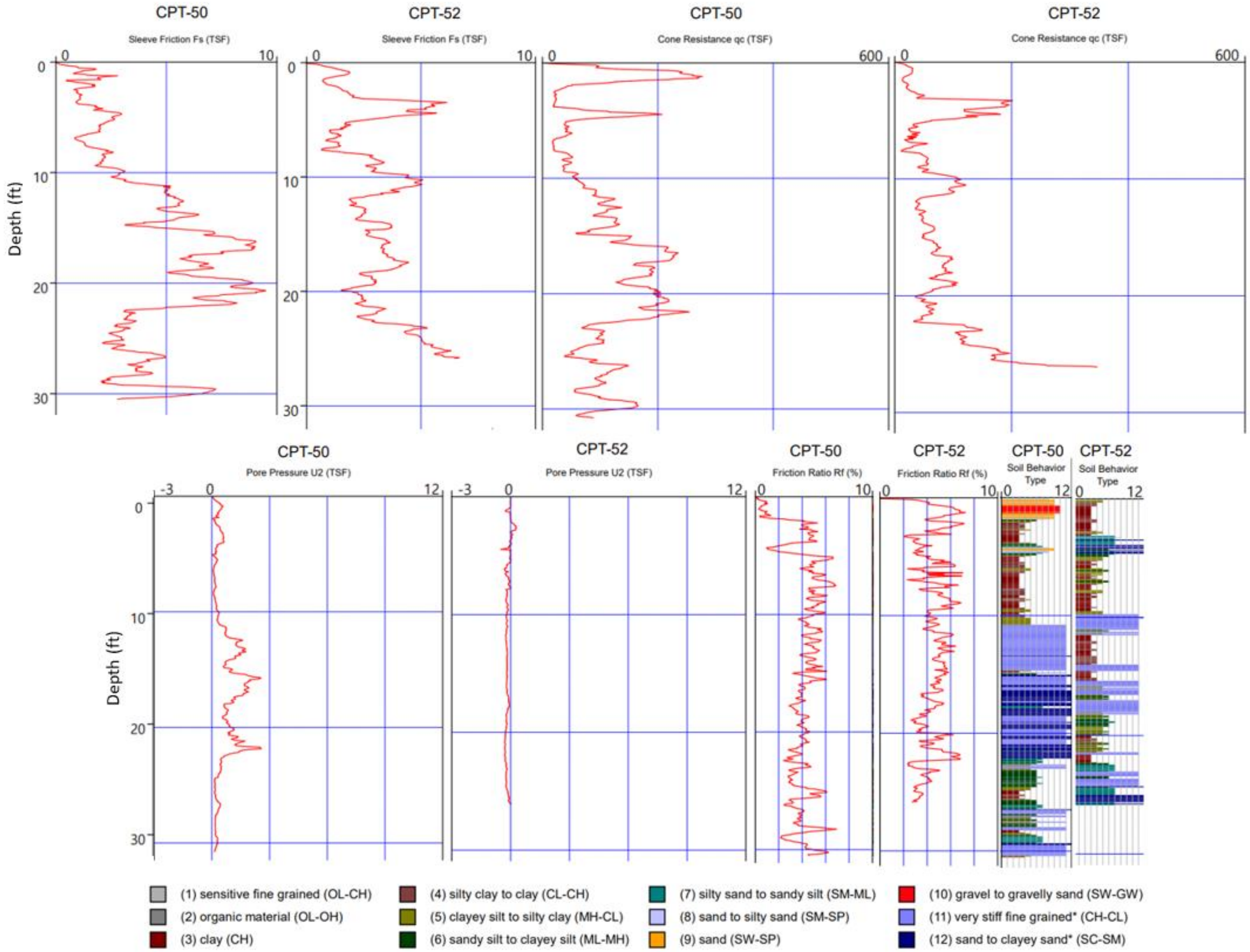

Figure 9: Side-by-side comparison of CPT-50 and CPT-52 profiles interpreted from the CPT software. The x-axis for the soil behavior type profiles are the 12 original soil behavior types[18].

Table 5: Condensed soil types based on the two Robertson et al. classifications[17,18] and interpreted hydraulic conductivity (K) and soil groups from this study.

Condensed Soil Types					
Robertson et al. (1990)	Robertson et al. (2010)	Unit[16]	K (m/s)	This Study: Categorical Hydraulic Conductivity	This Study: Similar Hydraulic Conductivity Soil Groups
1	1	Sensitive Fine Grained Soil	10^{-10} - 10^{-8}	Low	2
2	2	Fine Grained Soil	10^{-10} - 10^{-8}	Low	2
3	3	Clay	10^{-10} - 10^{-9}	Very Low	1
4	4	Silts	10^{-9} - 10^{-7}	Low	2
5					
26	5	Silty Sand	10^{-7} - 10^{-5}	Medium	3
7					
8	6	Sand	10^{-5} - 10^{-3}	High	4
9	7	Gravely Sand	10^{-3} - 1	Very High	5
10					
11	8	Dense Stiff Soil	10^{-8} - 10^{-3}	Medium	3
12	9	Stiff Fine Grained Soil	10^{-9} - 10^{-7}	Low	2

4.2 Correlation of Hydraulic Conductivity Values Using Lithology Models

Figure 10 shows the Rockware-interpolated materials, simplified into five categories (Table 5), across Area 3. Category 1 was originally labeled "fine grained organics" as interpolated by the CPT software, but organics are very rare in residuum or saprolite, and that category was changed to fine grained soil. Figure 11 shows 3-D fences across the site of the material overlying the bedrock. Figure 12 shows a cross-section of the distribution of pore pressures across the site. A high pore pressure indicates the presence of low hydraulic conductivity materials around the cone and that the pressure increase dissipated slowly while a low pore pressure indicates the presence of higher hydraulic conductivity materials around the cone and a faster pressure disipation. From Figures 10 and 11, there is evidence of lateral connectivity amongst layers, but not in the direction of dip, which does not support the first hypothesis. The bedrock dips to the south and the water table also deepens to the south. Denser material, such as from clay and very stiff fine-grained soils, had low hydraulic conductivity values and were confining units [29]. In the southern end of Area 3, hydraulic conductivity increased at depth and lithologic units were separated by clay-like material that could be impeding flow[19]. There was more shallow clay in the northern region[30]. Clay, silty sand, and dense stiff material near wells FW010 (which was screened at 5.71 m), FW134-2 (screened at a 8.7 m), and FW103 (screened at 11.78 m) had hydraulic conductivities determined from CPT pushes that ranged from 10^{-10} to 10^{-3} m/s, but the slug test hydraulic conductivity calculations for those three wells (Figures 13 – 15, respectively) ranged from 10^{-6} to 10^{-5} m/s (Table 5). Hvorslev curves for slug tests in the other wells are included as Figures 16-18. The range of CPT-estimated hydraulic conductivities was found to be wider than previous studies while the calculated hydraulic conductivities from the slug tests suggested a similar range to previous studies. Hydraulic conductivity values indicative of sand and gravely sand were calculated for deep saprolite in the southern portion of Area 3 (Table 5), which supports hypothesis three that the deep, weathered saprolite will have higher hydraulic conductivity values than the shallow saprolite.

4.3 Groundwater Flow from the Colloidal Borescope

The colloidal borescope was used to measure groundwater flow velocity and direction.

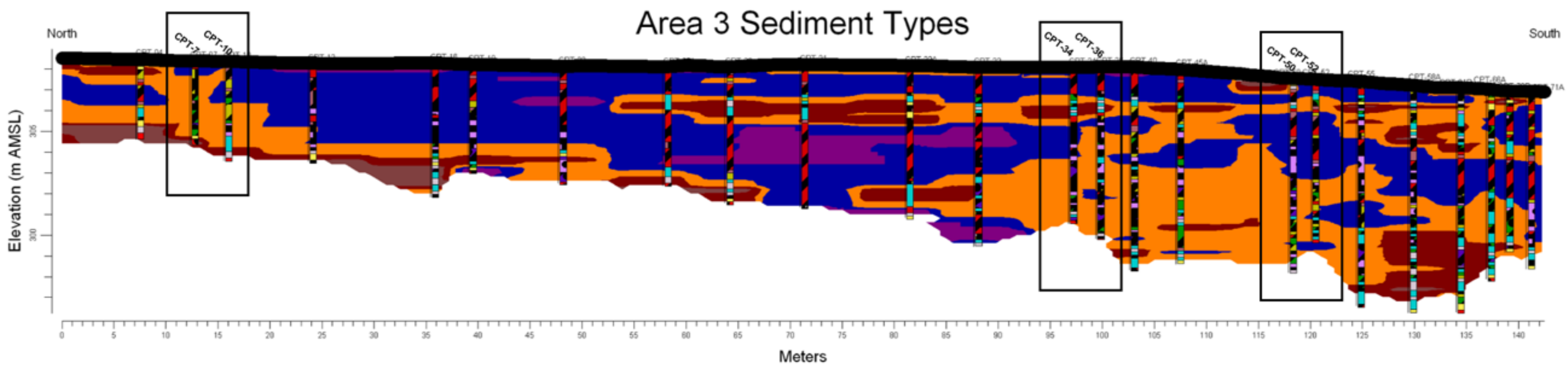

Legend		
Color	**Soil Type**	**Hydraulic Conductivity (m/s)**
	Clay (1)	$10^{-10} – 10^{-9}$
	Fine Grained Soil (2)	$10^{-10} – 10^{-8}$
	Silty Sand and Dense Stiff Soil (3)	10^{-8} - 10^{-3}
	Sand (4)	10^{-5} - 10^{-3}
	Gravely Sand (5)	10^{-3} - 1

Figure 10: North to south cross-section of Area 3, showing the Rockware-interpolated distribution of the different soil types based on the CPT profiles and interpreted hydraulic conductivity ranges. The numbers in parentheses in the legend refer to the condensed soil groups (Table 5). The interpolation occurs slightly above where refusal was hit for each push. The outlined boxes on the cross-section indicate the locations of the three pairs of CPT pushes shown in Figures 7, 8, and 9. There are more soil types with higher hydraulic conductivities in the southern portion of Area 3.

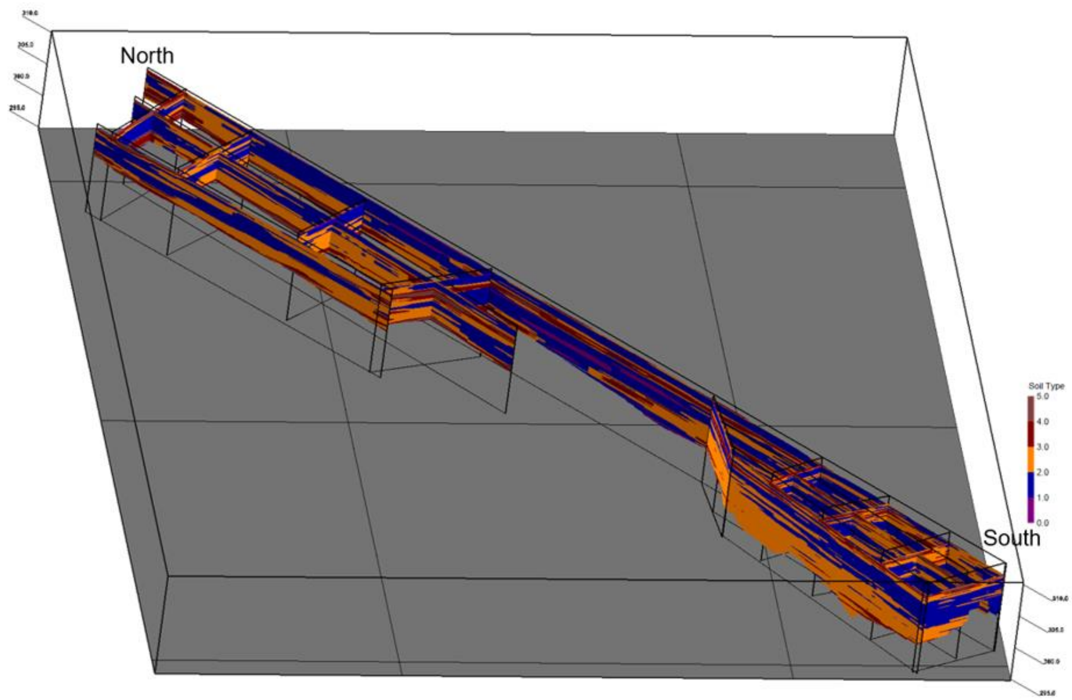

Legend		
Color	Soil Type	Hydraulic Conductivity (m/s)
	Clay (1)	$10^{-10} – 10^{-9}$
	Fine Grained Soil (2)	$10^{-10} – 10^{-8}$
	Silty Sand and Dense Stiff Soil (3)	10^{-8} - 10^{-3}
	Sand (4)	10^{-5} - 10^{-3}
	Gravely Sand (5)	10^{-3} - 1

Figure 11: 3-D fence representation of the length of Area 3, showing the Rockware-interpolated distribution of the different soil types and based on CPT profiles and soil classification according to hydraulic conductivity (Table 5).

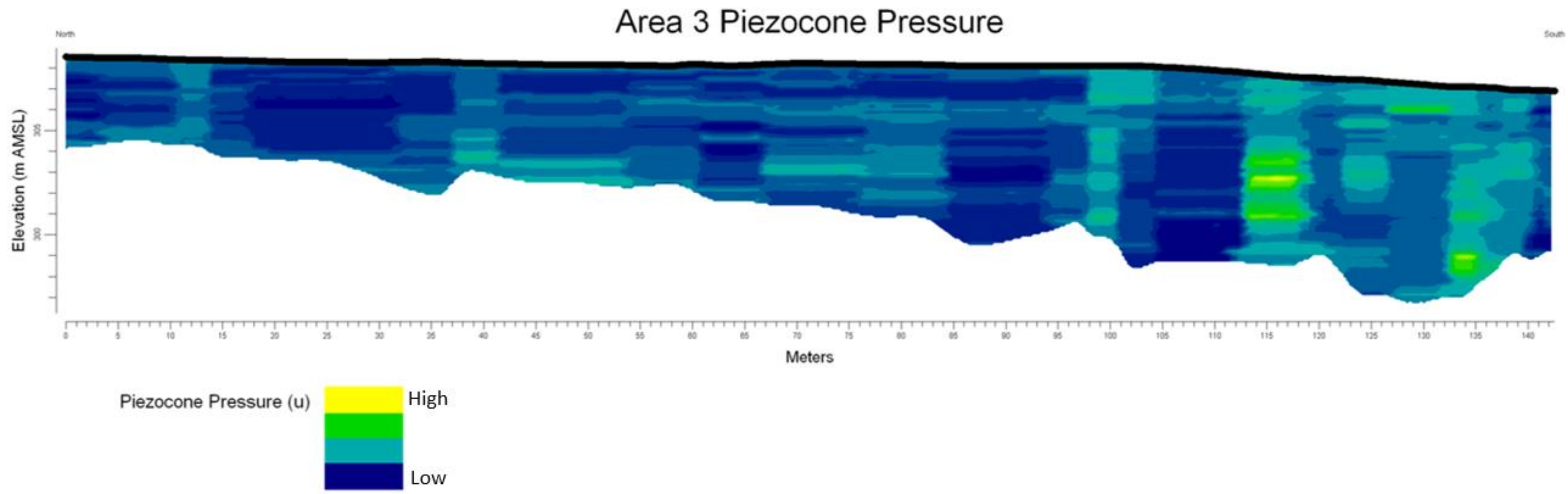

Figure 12: North to south cross-section of Area 3, showing pore pressure distribution. Pore pressure is higher in the deeper and southern portion of Area 3, indicating denser material.

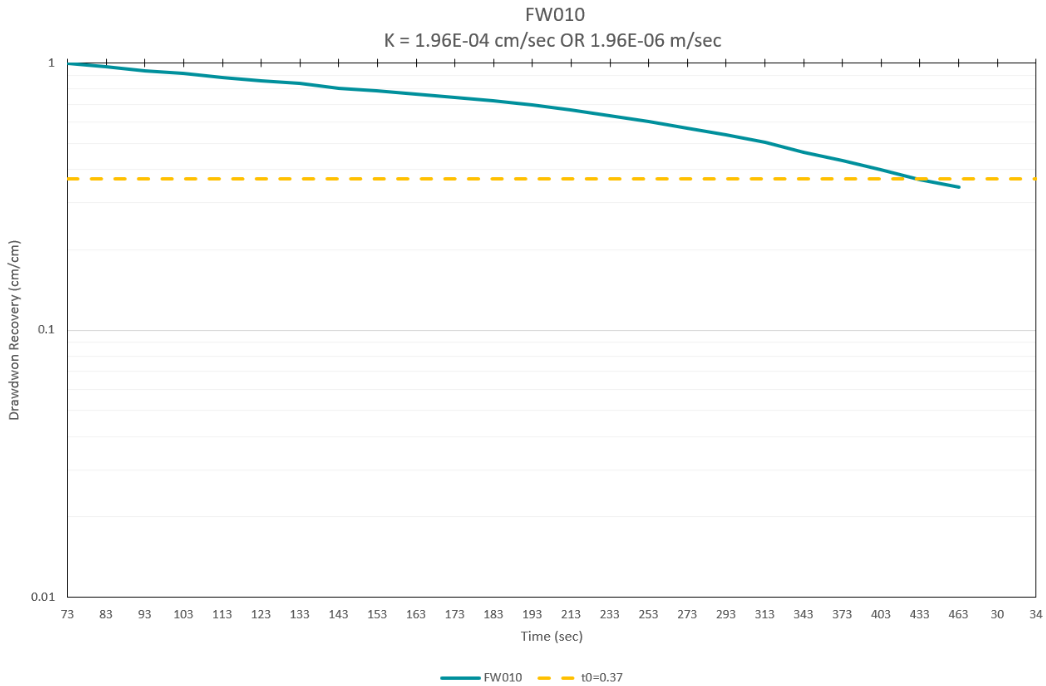

Figure 13: Drawdown/Recovery plot for calculating hydraulic conductivity in FW010 using the Hvorslev method.

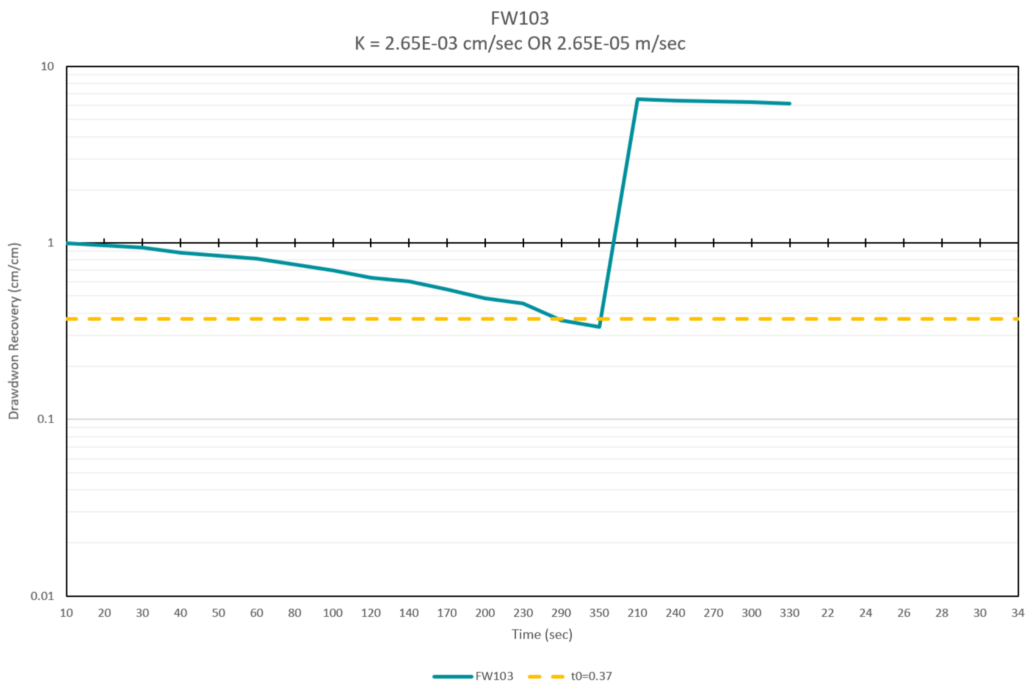

Figure 14: Drawdown/Recovery plot for calculating hydraulic conductivity in FW103 using the Hvorslev method. A large step increase after the time lag occurred when the slug was pulled out of the hole.

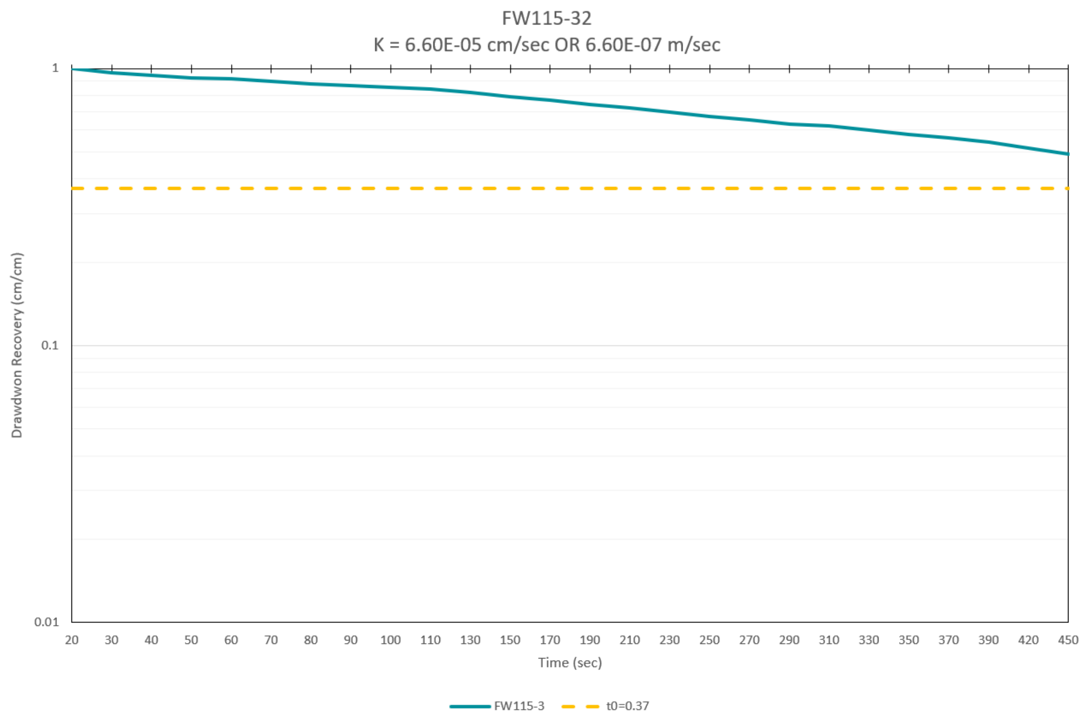

Figure 15: Drawdown/Recovery plot for calculating hydraulic conductivity in FW115-32 using the Hvorslev method.

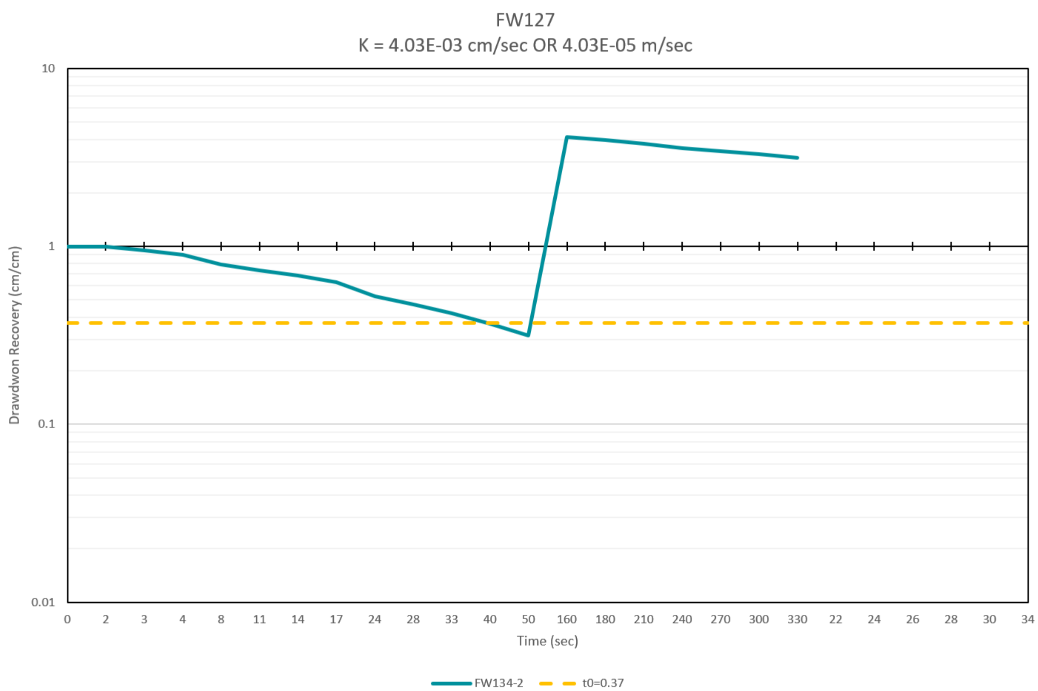

Figure 16: Drawdown/Recovery plot for calculating hydraulic conductivity in FW127 using the Hvorslev method. A large step increase after the time lag occurred when the slug was pulled out of the hole.

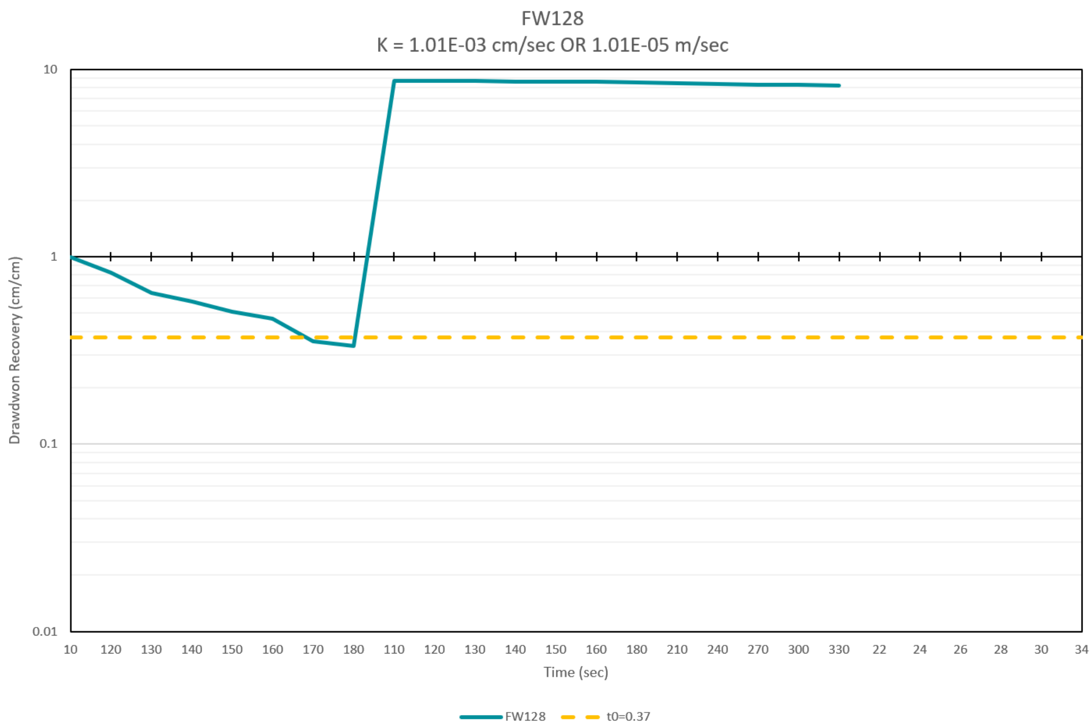

Figure 17: Drawdown/Recovery plot for calculating hydraulic conductivity in FW128 using the Hvorslev method. A large step increase after the time lag occurred when the slug was pulled out of the hole.

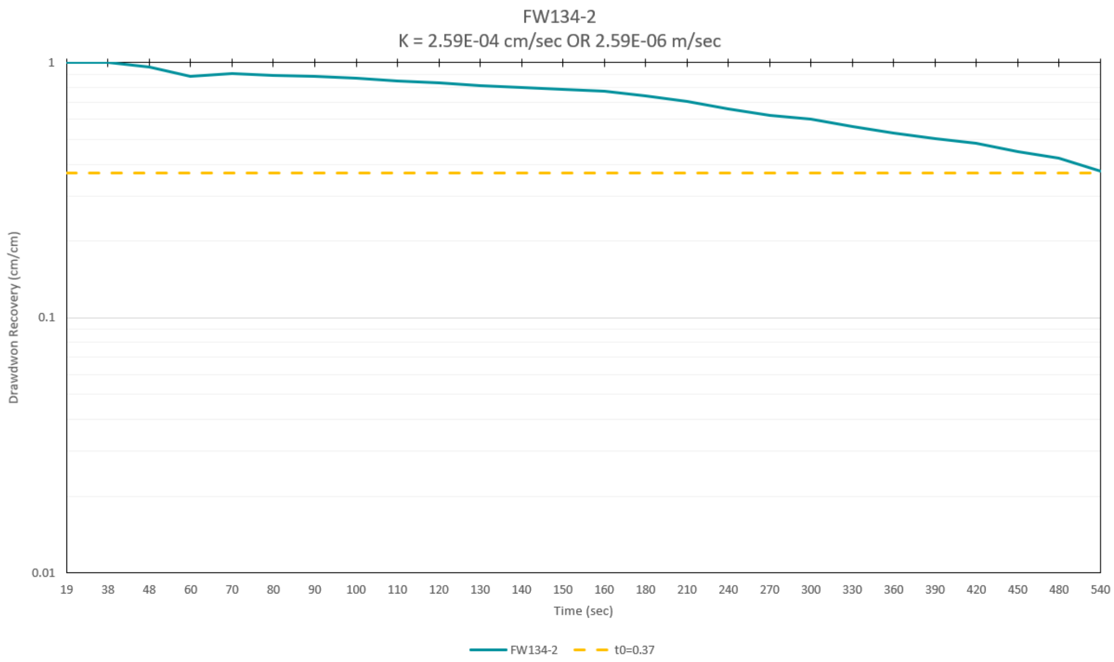

Figure 18: Drawdown/Recovery plot for calculating hydraulic conductivity in FW134-2 using the Hvorslev method.

Based on the measurements, groundwater flows in a southerly or southwesterly direction towards Bear Creek. A preferential flow zone was located at a depth between, generally, 12.2 and 12.5 m for these two deep wells. Figure 19 shows the flow vectors for FW127 and FW106 relative to where the wells are located. Both wells show groundwater flowing slightly southeast, and supported what the previous study found with well FW106 at a depth of 10.7 m [21]. Well FW127 had similar measurements, with the preferential flow zone located at a depth of 12.3 m (Figure 20). At this depth, the measured groundwater vector was 181.1 +/- 17.4 degrees south and the velocity was 15.3 +/- 7.8 m/day. The colloidal borescope measurements for well FW128 showed a preferential flow path at a depth of 12.8 m (Figure 21), and groundwater vector at 155.8 +/- 109.3 degrees south and a velocity of 15.1 +/- 12.1 m/day. Well FW128 had measurements with a constant velocity, but variable vectors. The velocity of the groundwater was constant, but because the direction vectors were constantly changing, it suggested that the colloidal borescope was at a depth that was either just above or just below where a preferential flowpath may be located. The colloidal borescope was picking up on that movement, but because it was not directly in the flowpath, the water was forced to go around the borescope and show up as flow vectors that kept changing direction.

4.4 Hydraulic Conductivity and Water Table Measurements

Hydraulic conductivities were determined from slug tests (Table 5) and groundwater flow measurements were taken using the colloidal borescope for Area 3. The hydraulic conductivities ranged from 6.6×10^{-7} m/sec (equivalent to silt or silty sand[16]) to 4.03×10^{-5} (equivalent to silty sand or sand[16]) m/sec, or 0.06 to 3.5 m/day. Lower hydraulic conductivity values were calculated for wells located from the middle to north of Area 3, specifically wells FW010, FW134-2, and FW103.

During CPT tests, water table measurements were recorded by Level TROLLs (Figure 22). Water table measurements ranged from about 3.0 to 4.6 m below ground surface. Depth to water measurements were shallower in the north and deeper in the south because of the dip of the

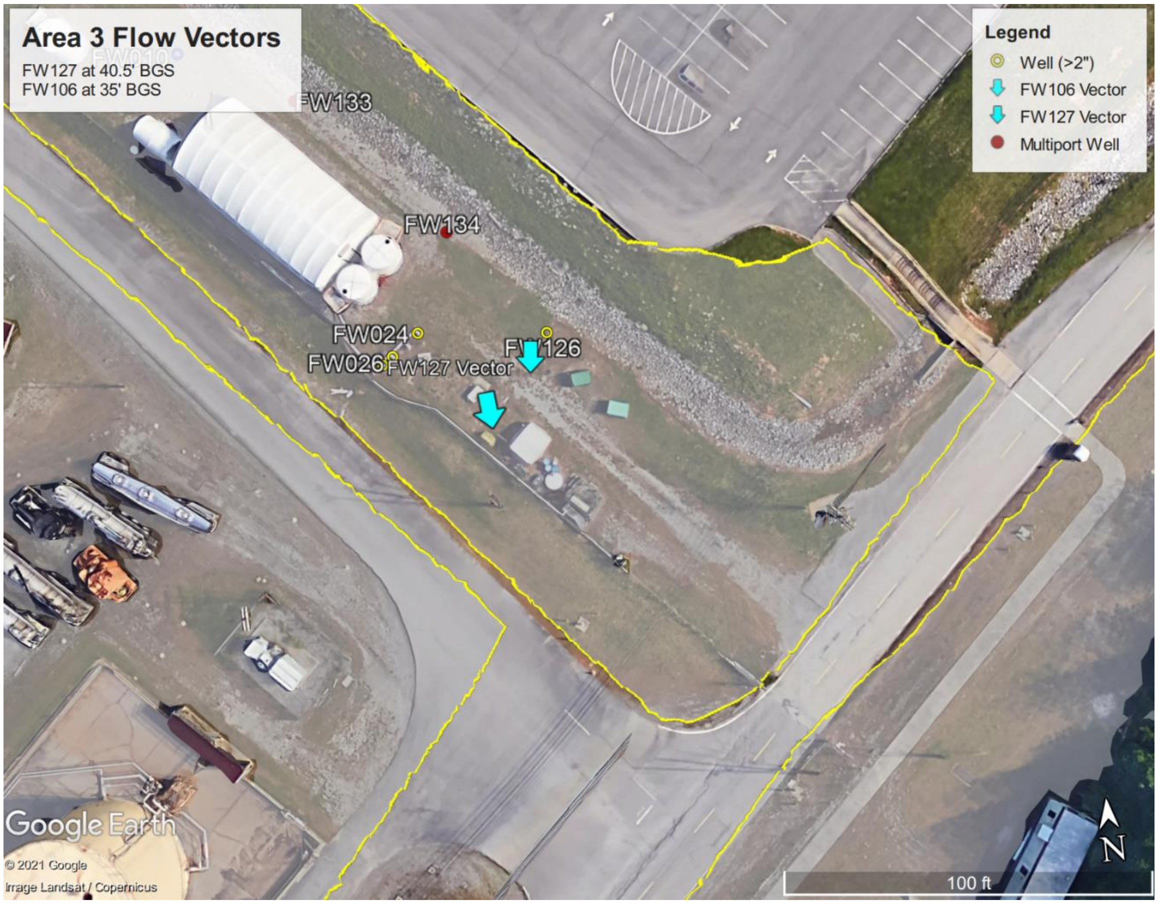

Figure 19: Area 3 map with the direction of flow vectors in wells FW127 (this study) and FW106 (previous ENIGMA study) determined by the colloidal borescope measurements. The flow vectors show groundwater flowing to the southern corner of Area 3, Oak Ridge, TN.

Image location, 35° 58’ 37.82”N, 84° 16’ 23.73”W, eye alt 259 feet. Image taken from Google Earth, http://earth.google.com, Image Landsat/Copernicus (V 7.1., accessed November 9, 2019).

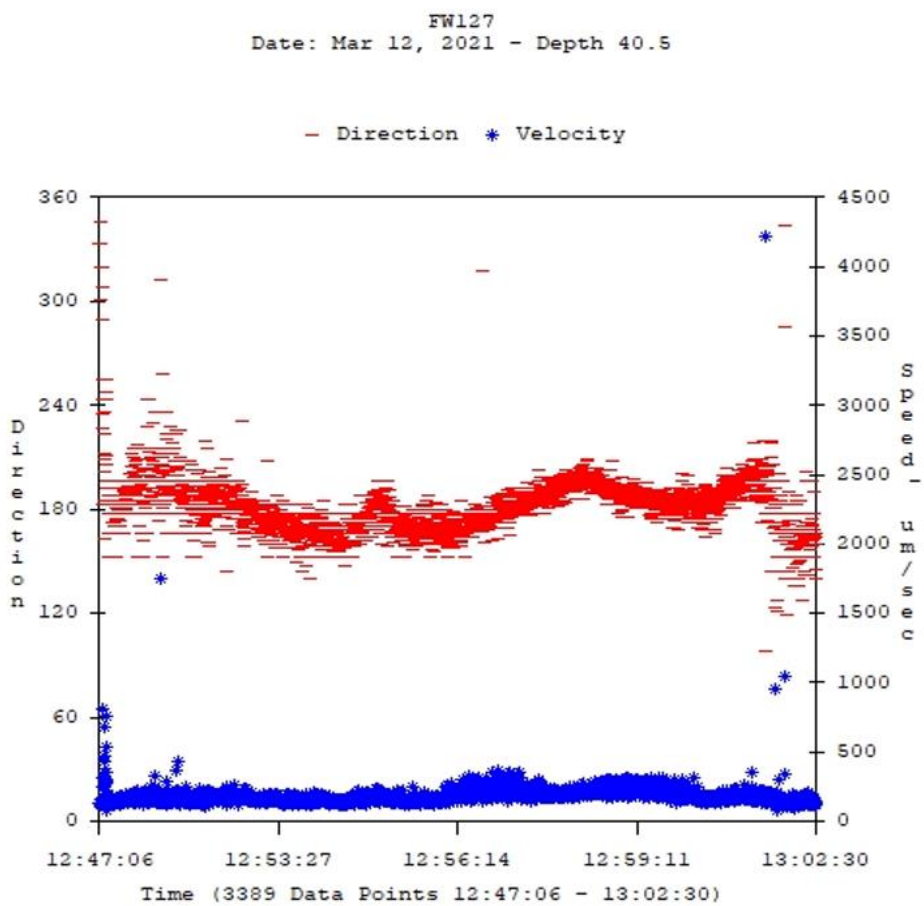

Figure 20: The results of the colloidal borescope measurements for well FW127. Velocity is blue and direction is red. The direction and velocity vectors were stable at this depth in well FW127, which indicated a preferential flow zone.

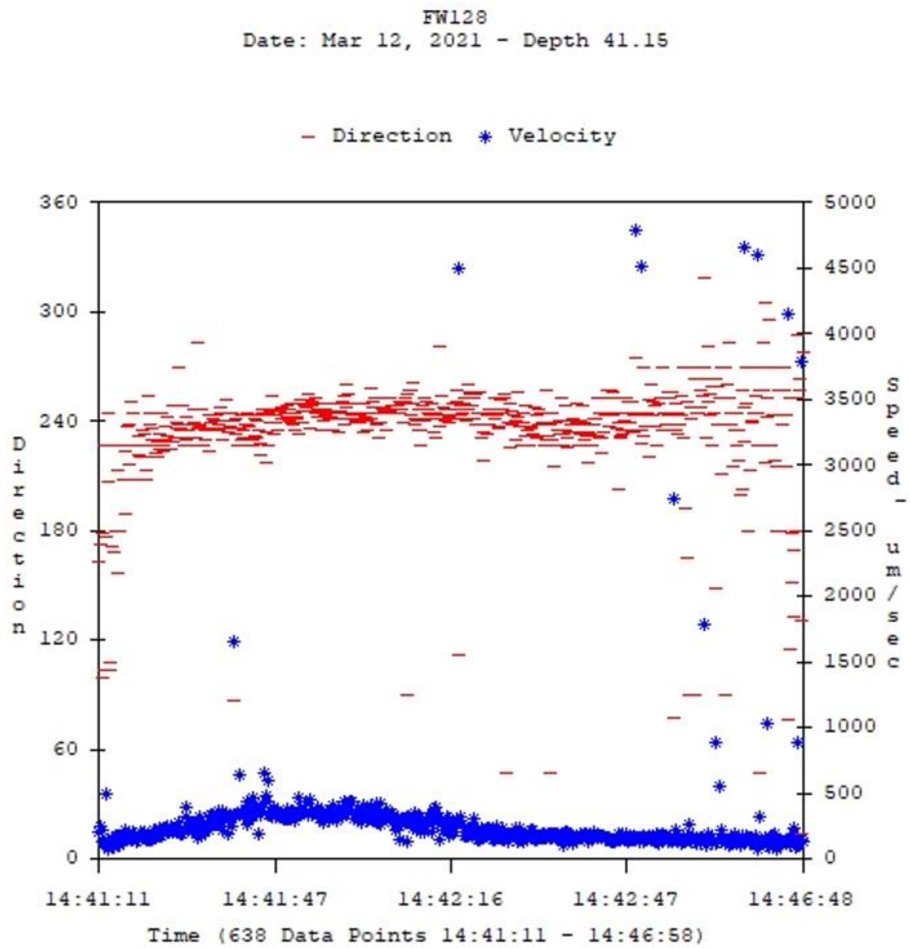

Figure 21: The results of the colloidal borescope measurements for well FW128. Velocity is blue and direction is red. The direction and velocity vectors were not stable at this depth, which indicated that either the instrument mixed up particles in the water too much or this was a depth either just above or below the preferential flow zone.

bedrock[9]. This creates a hydraulic gradient that indicated groundwater is flowing to the south towards Bear Creek. The water table measurements were used to calculate the hydraulic head values and estimate where the water table was located[31]. Hydraulic gradients were determined from the well data and assumed hydraulic conductivity was equal in all directions. The flow directions from the hydraulic gradient data are like the directions determined from the colloidal borescope measurements.

4.5 Nitrate Concentrations and Geochemical Comparisons

Geochemistry measurements during well purging and sampling included temperature, pH, conductivity, and dissolved oxygen. Dissolved oxygen values ranged from 1.39 mg/L to 0.01 mg/L (Table 7). Although alkalinity was measured for the groundwater samples collected from each of the wells, wells FW010, FW126, FW106, FW128, and FW127 had alkalinity measurements of 0 mg/L as bicarbonate (HCO_3^-) (Table 7). The other wells had low alkalinity measurements, but well FW133-1 had the highest value. This well also had the highest nitrate concentration (Table 6). Along with well FW010, these two wells were the furthest north in Area 3 and were screened to the shallowest depths (Table 2). One shallow and one deep well had low nitrate concentrations. From these data, hypothesis four appeared to not be supported because both high and low nitrate concentrations were found in wells with similar hydraulic conductivity values. This indicates that there is little to no relationship between nitrate concentration and hydraulic conductivity. Lower pH values corresponded to higher conductivity values. A Spearman correlation was done to compare the geochemical parameters to nitrate concentrations with a critical value of ±0.65 (Figure 23). Nitrate was positively correlated with magnesium, nitrite, chloride, calcium, and the conductivity measurements. Moreover, nitrate was negatively correlated with dissolved oxygen. Based on the correlation results, a statistically significant regression model ($P < 0.05$) and its residuals indicated that conductivity and calcium were the most correlated to nitrate concentrations across the site (Figures 24 and 25).

Table 6: Hydraulic conductivities and nitrate concentrations for each applicable well.

Well	Hydraulic Conductivity From Slug Test (m/s)	Nitrate (mg/L)
FW010	2.0×10^{-6}	19,794
FW024	N/A	5,870
FW026	N/A	0.3
FW103	2.7×10^{-5}	985
FW106	N/A	1,829
FW126	N/A	7,098
FW127	4.0×10^{-5}	2,989
FW128	1.0×10^{-5}	5,083
FW133-1	$>2.8 \times 10^{-6}$ [1]	36,676
FW134-2	2.6×10^{-6}	0.2
FW115-32	6.6×10^{-7}	N/A

[1]Well responded too quickly to measure slug test so minimum value was calculated by using time it took to drop slug and write first water level measurement

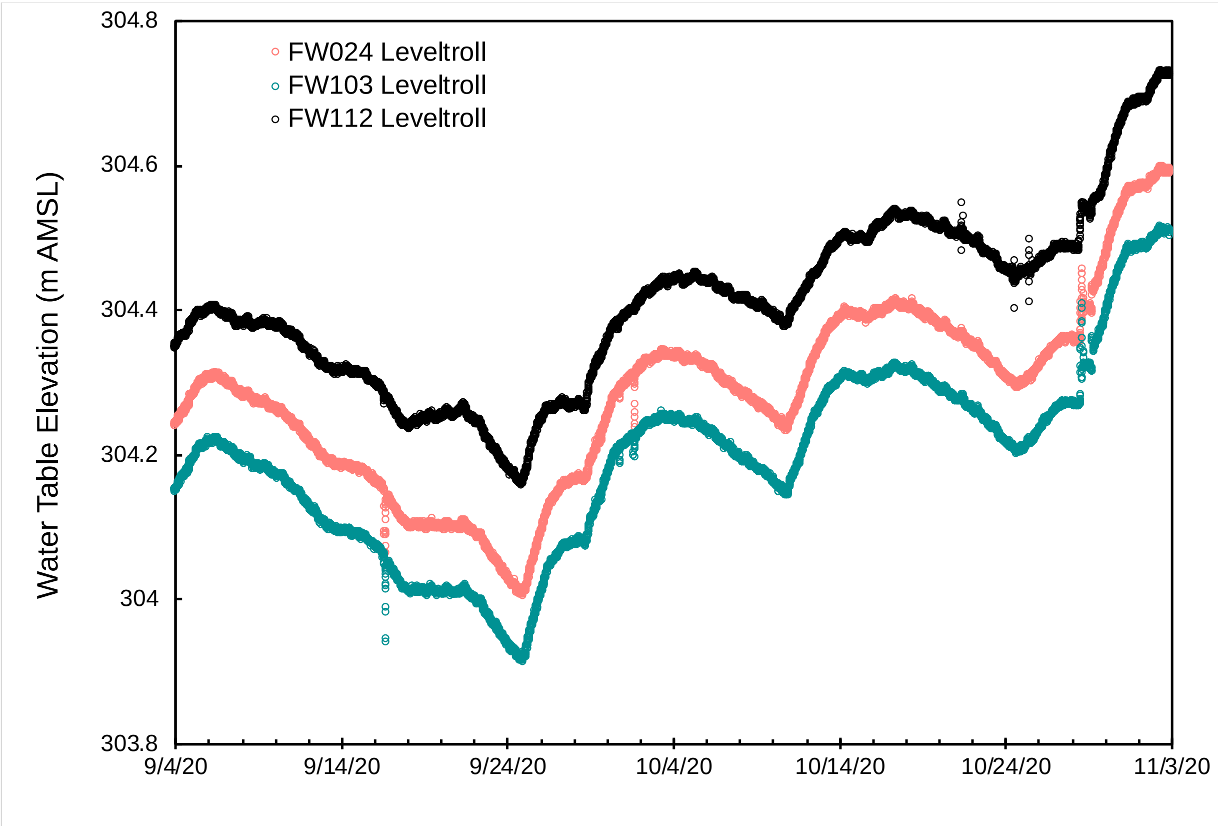

Figure 22: Water level data for wells FW024, FW103, and FW112 collected from September to November in 10-minute intervals. Local CPT activities occurred on 2020-10-18, 2020-10-20 – 2020-10-22, 2020-10-24, and 2020-10-25. Observable water level variation was exhibited in FW112 from local CPT activities on 2020-10-21, 2020-10-22, 2020-10-24 and 2020-10-25. On 2020-10-28, the site received 5.2 centimeters of rain and an additional 2.5 centimeters on 2020-10-29, resulting in the rising water levels after 2020-10-28[20].

Table 7: Geochemical parameters arranged by flow path, with "1" referring to the shallow flow path and "2" referring to the deeper flow path (Table 2).

Well	Flow Path	Temperature (°C)	pH	Conductivity (μS/cm)	Na (mg/L)	K (mg/L)	Mg (mg/L)	Ca (mg/L)	F (mg/L)	Cl (mg/L)	NO_2 (mg/L)	NO_3 (mg/L)	SO_4 (mg/L)	PO_4 (mg/L)	HCO_3 (mg/L)	O_2 (mg/L)
FW010	1	20.62	3.76	21450	689.1	111.7	489.57	3941.33	84.34	286.45	8.21	19793.61	1.37	4.91	0	0.01
FW133-1	1	20.02	5.32	21470	879.1	86.21	967.38	8967.23	0.74	419.51	87.24	36676.12	2.05	0	380.4	0.03
FW134-2	1	19.64	6.22	391.9	19.01	6.14	8.06	48.03	1.75	14.36	0.04	0.22	256.4	0.04	92.23	1.39
FW126	2	20.51	3.43	11330	918.87	82.39	97.43	837.51	3.37	339.74	1.2	7098.34	1285.15	1.1	0	0.01
FW106	2	25.09	4.04	6038	824.46	138.46	25.93	203.38	20.76	238.26	1.71	1828.76	1499.62	0.65	0	0.11
FW128	2	23.83	3.82	9808	885.53	221.04	64.36	666.55	1.66	266.01	2.6	5082.72	1226.41	0.12	0	0.07
FW127	2	20.08	3.76	6666	965.72	43.72	36.09	318.39	23.1	262.85	2.59	2988.98	1364.25	0.54	0	0.05
FW103	2	21.16	5.26	2001	82.36	39.96	32.06	246.59	9.89	81.21	0.4	984.82	174.41	0	60.76	0.25
FW026	2	24.09	6.09	1214	46.14	21.27	15.62	113.64	1.84	42.41	0.12	0.29	84.65	2.24	72.71	0.13
FW024	2	20.99	4.51	8597	350.54	51.54	121.02	1200.03	17.08	187.61	17.83	5870.46	273.47	0	45.87	0.1

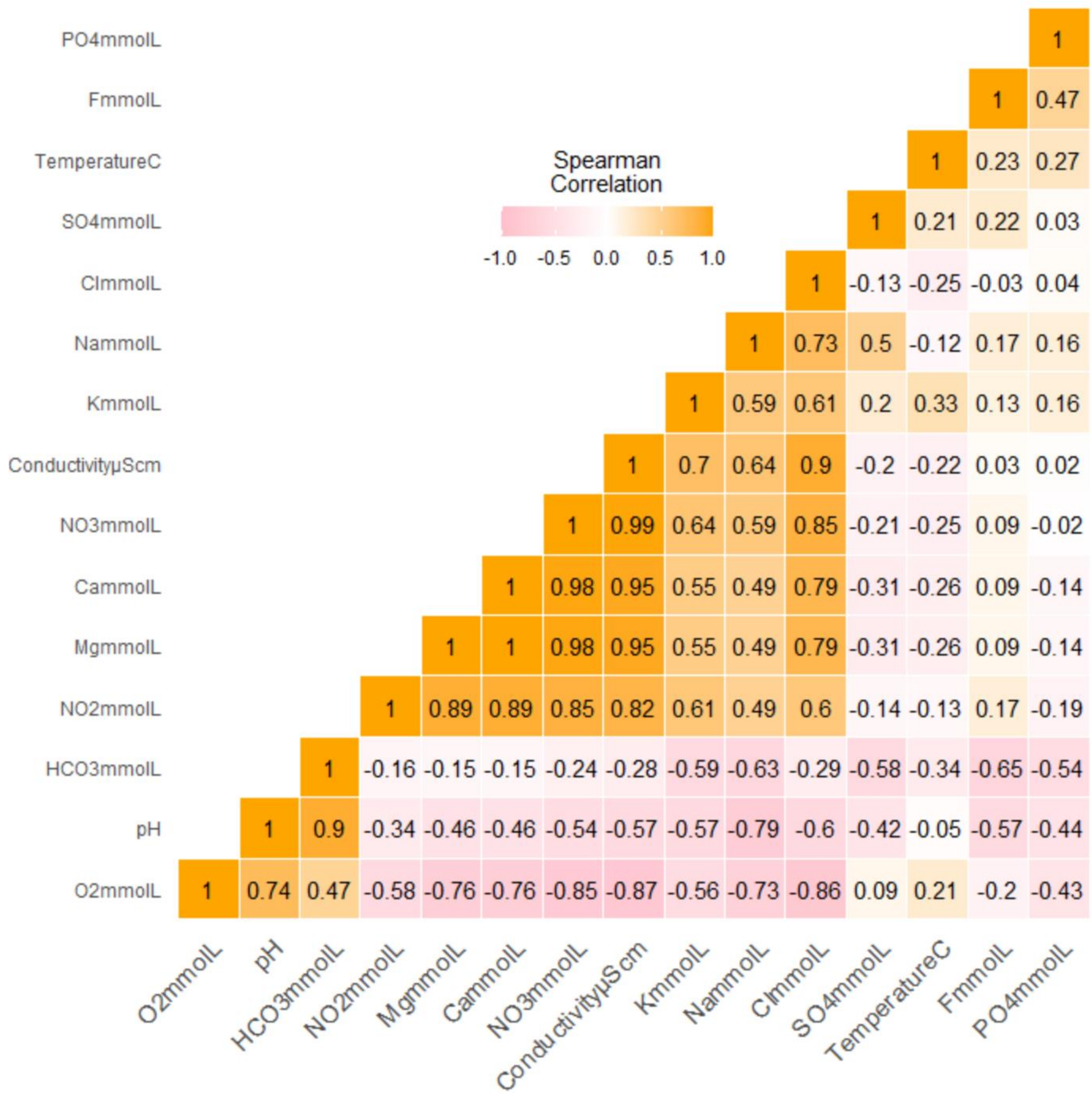

Figure 23: Spearman test results evaluate nitrate concentration and other geochemical parameters. Pink indicates a negative correlation and orange indicates a positive correlation (P<0.05 = r = ±0.65). White or light shades of pink and orange indicate little to no correlation between geochemical parameters.

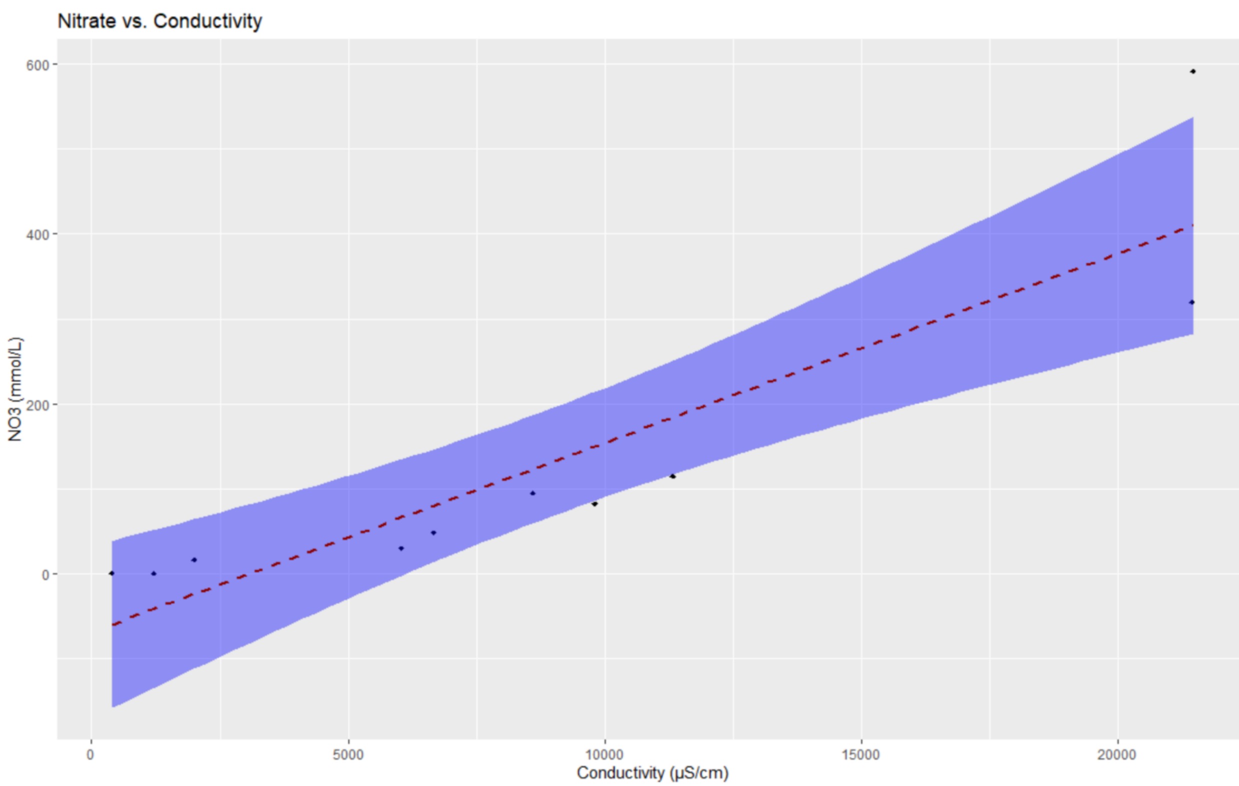

Figure 24: The regression model for the relationship between nitrate and conductivity. The dashed line is the linear trend line, and the blue shaded region represents the 95% confidence interval. The black dots are the measurements that were taken.

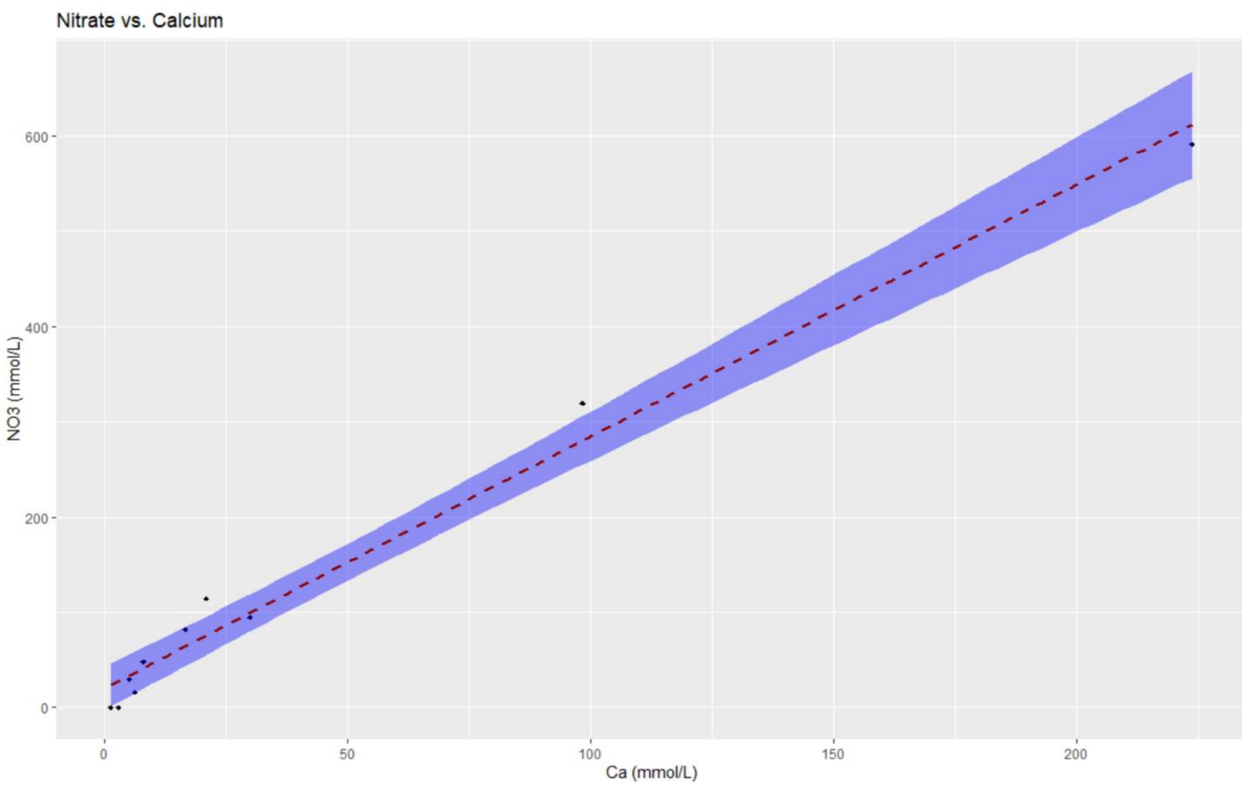

Figure 25: The regression model for the relationship between nitrate and calcium. The dashed line is the linear trend line, and the blue shaded region represents the 95% confidence interval. The black dots are the measurements that were taken.

Chapter 5 Discussion

Despite past research efforts to understand contaminant transport in the weathered materials at uncontaminated ORR sites, there has been limited research conducted at contaminated sites, and relatively little information on how geological material properties, especially hydraulic conductivity values in the saprolite, control the distribution of contaminants. The main goals of this study were to (i) measure the variability of physical and hydrogeological properties in the weathered materials (i.e., saprolite) at Area 3, (ii) determine how the physical and hydrogeological properties control the distribution of nitrate contamination from the S-3 pond, and (iii) assess nitrate and geochemical correlations, which could provide insight into nitrate transformation processes. These goals were achieved by meeting four objectives and testing four hypotheses (see Chapter 2).

5.1 Lateral Connectivity of Weathered Material Properties

This study, which was the first to use CPT at the S-3 ponds site, was the most detailed shallow subsurface characterization of Area 3 to date. Hypothesis one states that the highly weathered materials overlying bedrock in Area 3 will show substantial lateral connectivity along the direction of the bedding (i.e., dipping to the southeast). The profiles from the CPT data show lateral connectivity, with generalized soil types located adjacent to each other within a few meters. However, lateral connectivity does not follow the direction of the dip of bedding and is instead horizontal[12]. This suggests that physical properties of the saprolite are more strongly impacted by depth of weathering, than by structure of the parent bedrock. It also suggests that the shallow weathered material may resemble the residuum typically developed from carbonate bedrock rather than saprolite, which is typically developed from shale. This may include differences in the lithology of the parent bedrock (i.e., interbedded layers of shale and limestone), but this can be difficult to see via CPT. The colloidal borescope measurements found that the preferential flow zone for wells FW127 and FW128 is between 12.2 and 12.8 m below ground surface and that the groundwater flow vector is between 155 and 181 degrees south. This flow zone falls where there is a large Rockware-interpreted silty sand and dense stiff soil section in the cross section (Figure 10). Wells FW103, FW026, FW024, and FW106 are also located in this soil type and are screened to that depth or deeper so they could possibly be a part of this flow zone as well.

The preferential flow zone is at a similar depth for the wells in flow path two (Table 7), which may support the idea of lateral connectivity between adjacent soil types. Depth to the water table was slightly shallower in the northern section of Area 3 compared to the southern section. This is because of the dip of the bedrock. Water cannot easily infiltrate the intact bedrock that is closer to the ground surface in the north, which causes a slight gradient to the south. The bedrock interface is shallower in the north than the south because of CPT refusal depths and previous drilling refusals when wells were installed.

5.2 Hydraulic Conductivity Investigations

Hypothesis two states that hydraulic conductivity estimated from CPT profiles will correspond with zones of higher hydraulic conductivity measured in nearby wells (Table 1) using slug tests. Wells FW127, FW128, and FW103 had the highest hydraulic conductivity values calculated from the slug tests (Table 6). FW127 and FW128 are located near CPT-50 and CPT-52. The material that corresponds with the screened interval depth for these pushes is in the silty sand and dense stiff soils, with a hydraulic conductivity range of 10^{-8} – 10^{-3} m/s. Well FW103 is located nearest to CPT-34 and CPT-36. It had a hydraulic conductivity value of 2.65 x 10^{-5} m/s and the material that corresponded to the screened interval for those pushes was the silty sand and dense stiff soils, as well. A paired t-test found that the hydraulic conductivities calculated from the slug tests were not significantly different from the hydraulic conductivities of the materials that the pushes near those wells. It is possible that the material at the same depth as the screened interval of nearby wells, and only a few meters away, could be interpreted as having similar hydraulic conductivities, which may support lateral connectivity between soil types and preferential flow zones.

The third hypothesis states that the deep saprolite will have higher hydraulic conductivity values compared to the shallow saprolite. The shallow-screened wells that had slug tests performed (FW010 and FW134-2), had hydraulic conductivity values of 2.0 x 10^{-6} and 2.6 x 10^{-6} m/s, respectively. The deep-screened wells that had slug tests performed (FW127, FW128, and FW103) had hydraulic conductivities in the 10^{-5} m/s range. The cross-section (Figure 10) shows that there is more silty sand and dense stiff soils and sand materials in the southern portion of Area 3 where the deeper saprolite is compared to the northern region where the shallow saprolite is located. This means that the deep saprolite does have slightly higher hydraulic conductivity values than the shallow saprolite. The values are only different by an order of magnitude, which is not large in terms of hydraulic conductivity ranges. A previous study stated that there was a difference in hydraulic conductivity between shallow and deep saprolite by a couple orders of magnitude and the range of values didn't match what this study found[9]. That study wasn't as high of a resolution as this one and the wells that were measured weren't the same as the ones in this study. A more recent study found that the range of hydraulic conductivity values for the saprolite was similar to what was found in this study[13]. This study used a site upgradient from the S-3 ponds to collect their saprolite samples, but our study used Area 3 adjacent to the S-3 ponds.

Hydraulic conductivity values were highest in the shallow saprolite and this was supported by a previous study at a site in similar materials, located outside the Oak Ridge Reservation[2]. A different study found that low hydraulic conductivity values correspond to the disappearance of soil structures and an increase of infilling of macropores with clays and Fe/Mn oxides[7]. This study found through CPT interpretation that there are clay layers throughout Area 3 and these zones of clay have lower hydraulic conductivities than the other soil types. Hydraulic conductivity values vary significantly by depth indicating that lithology is a control. Alternating layers of high and low hydraulic conductivity are estimated based on substantial variation in values from the CPT results. Hydraulic conductivity is controlled by fractures, dissolution, matrix diffusion, and seasonal variability in the shallow subsurface of Area 3. Fractures and dissolution of carbonate minerals along flow paths can create zones of higher hydraulic conductivity in regions with lower hydraulic conductivities. Precipitation and temperature can affect the hydraulic conductivity of the shallow subsurface. Clays may dry and fracture during periods of drought and high heat resulting in larger hydraulic conductivities than during a wet and cool time[32]. Hydraulic conductivity values calculated from both slug tests and estimated through CPT interpretation are controlled by many different factors in the saprolite, which helps to explain the range of values at the same depth across the site.

5.3 Nitrate Correlations and Transport

Nitric acid is the source of nitrate in the former S-3 waste ponds. The fourth hypothesis states that nitrate concentrations are expected to be higher in zones of lower hydraulic conductivity, as estimated by CPT data or measured using slug tests in wells. The second highest nitrate concentration, ~19,793 mg/L, was found in well FW010, which had a lower hydraulic conductivity, 2.0 x 10^{-6} m/s (Table 6), and was in a zone of lower hydraulic conductivity values in the northern part of Area 3. The lowest nitrate concentration, ~0.22 mg/L, was in well FW134-2, which had a similar hydraulic conductivity value to FW010 at 2.6 x 10^{-6} m/s (Table 6). Because the highest and lowest nitrate concentrations were in wells that had almost identical hydraulic conductivity values, there does not appear to be a relationship between nitrate concentration and hydraulic conductivity. However, higher nitrate concentrations were generally recovered where there was higher clay content (Figure 10) and from wells with lower hydraulic conductivity values, which implies that slow flow may be impeding the movement of nitrate. In contrast, low nitrate concentrations were recovered where hydraulic conductivity values were higher, which would result in higher rates of flushing in fractures and lenses of permeable soil types. Higher nitrate concentrations are also found where sulfate concentrations were low , and when dissolved oxygen was low or absent[33].

Consequently, nitrate transport across Area 3 is not only controlled by material hydraulic conductivity but also microbial processes. Nitrate contamination should generally follow the flow of groundwater south towards Bear Creek. There are exceptions because nitrate persists at higher concentrations, and the groundwater in these zones is likely in a state of sulfate reduction or methanogenesis.

Chapter 6 Conclusions and Future Work

This study measured the variability of physical and hydrogeological properties in the saprolite at Area 3, determined how the physical and hydrogeological properties control the distribution of nitrate contamination from the S-3 ponds, and assessed nitrate and geochemical correlations to provide insight into nitrate transformation processes. Nitrate is important to study because the maximum contaminant level for drinking water is set by the US EPA at 10 mg/L. Although the groundwater at Area 3 will not be used as drinking water, the groundwater does flow in the direction of a surface creek, which could result in elevated nitrate levels over time. Transport of nitrate in the groundwater of Area 3 is controlled by hydraulic conductivity, which varied by depth due to bedrock lithology, fractures, dissolution, matrix diffusion, and seasonal conditions. Within the subsurface at Area 3, saprolite had laterally connected layers, and hydraulic conductivity values estimated by the CPT analyses corresponded to hydraulic conductivity values measured from slug tests in nearby wells. The deep saprolite generally had higher hydraulic conductivity values compared to the shallow saprolite, and hydraulic conductivity did not appear to correlate with nitrate concentration.

This study can help the understanding of other complex shallow aquifer systems that are contaminated with high concentrations of nitrate and other mixed waste. Legacy waste sites, like Area 3 and the S-3 waste ponds, may have prolonged contamination issues that require intensive engineering fixes because of the effects of the geology and hydrogeology on natural attenuation. To reduce nitrate contamination, amendments would be needed to increase the hydraulic conductivity or flow rate of the subsurface to flush the groundwater system. To use microbes to decrease nitrate concentrations, denitrification needs to be favored. Nitrate is likely persisting because of a combination of low hydraulic conductivity and the groundwater being in sulfate reduction or methanogenesis, in which case those microorganisms do not need nitrate. Additional slug tests at different depths could help to investigate other types of relationships between nitrate concentrations and hydraulic conductivity that could not be evaluated in this study. A future PHREEQC analysis for denitrification in Area 3 could also help to explain why nitrate is depleting so slowly. An additional lab analysis could be done for the 10 wells used in this study to identify the age of the groundwater flowing through the two flow paths. Lastly, a non-reactive tracer test could also be done to characterize reactive mass transport of nitrate in Area 3 for future iterations of the exploratory MT3D-USGS reactive transport model, as described in Appendix A.

References

1. Solomon, D. K.; Moore, G. K.; Toran, L. E.; Dreier, R. B.; McMaster, W. M. *Status Report: A Hydrologic Framework For The Oak Ridge Reservation*; Oak Ridge National Laboratory Publication: Oak Ridge, TN, 1992.
2. McKay, L. D.; Driese, S. G.; Smith, K. H.; Vepraskas, M. J., Hydrogeology and pedology of saprolite formed from sedimentary rock, eastern Tennessee, USA. *Geoderma* 2005**,** *126* (1-2), 27-45.
3. Jardine, P. M.; Wilson, G. V.; Luxmoore, R. J., Unsaturated solute transport through a forest soil during rain storm events. *Geoderma* 1990**,** *46* (1), 103-118. https://www.sciencedirect.com/science/article/pii/0016706190900107.
4. Lee, R. R.; Ketelle, R. H.; Bownds, J. M.; Rizk, T. A., Aquifer analysis and modeling in a fractured, heterogeneous medium. *Ground Water* 1992**,** *30* (4), 589-597.
5. Jardine, P. M.; Sanford, W. E.; Gwo, J. P.; Reedy, O. C.; Hicks, D. S.; Riggs, J. S.; Bailey, W. B., Quantifying diffusive mass transfer in fractured shale bedrock. *Water Resources Research* 1999**,** *35* (7), 2015-2030.
6. McKay, L. D.; Sanford, W.; Strong, J. M., Field-scale migration of colloidal tracers in a fractured shale saprolite. *Ground Water* 2000, *38*, 139-147.
7. McCarthy, J. F.; McKay, L. D.; Bruner, D. D., Influence of ionic strength and cation charge on transport of colloidal particles in fractured shale saprolite. *Environmental Science & Technology* 2002, *36* (17), 3735-3743. https://doi.org/10.1021/es025522o.
8. Hazen, T. C., Environmental Systems Biology Approach to Bioremediation. In *Understanding Terrestrial Microbial Communities*, Hurst, C. J., Ed. Springer International Publishing: Cham, 2019; pp 103-127.
9. Watson, D.; Kostka, J.; Fields, M.; Jardine, P. *The Oak Ridge Field Research Center conceptual model*; 2004. https://public.ornl.gov/orifc/FRC-conceptual-model.pdf.
10. Brooks, S. C. *Waste Characteristics of the Former S-3 Ponds and Outline of Uranium Chemistry Relevant to NABIR Field Research Center Studies*; United States, 2001, https://info.ornl.gov/sites/publications/Files/Pub57201.pdf.
11. Revil, A.; Skold, M.; Karaoulis, M.; Schmutz, M.; Hubbard, S. S.; Mehlhorn, T. L.; Watson, D. B., Hydrogeophysical investigations of the former S-3 ponds contaminant plumes, Oak Ridge Integrated Field Research Challenge site, Tennessee. *Geophysics* 2013, *78* (4), EN29-EN41. https://doi.org/10.1190/geo2012-0177.1.
12. Hatcher, R. D., Jr.; Lemiszki, P. J.; Foreman, J. L.; Dreier, R. B.; Ketelle, R. H.; Lee, R. R.; Lee, S. Y.; Lietzke, D. A.; McMaster, W. M. *Status report on the geology of the Oak Ridge Reservation*; United States, 1992; p 271. http://inis.iaea.org/search/search.aspx?orig_q=RN:24060945.
13. Revil, A.; Skold, M.; Hubbard, S. S.; Wu, Y.; Watson, D. B.; Karaoulis, M., Petrophysical properties of saprolites from the Oak Ridge Integrated Field Research Challenge site, Tennessee. *Geophysics* 2013, *78* (1), D21-D40.
14. Rogers, J. D., Fundamentals of cone penetrometer test (cpt) soundings. 2011, https://web.mst.edu/~rogersda/umrcourses/ge441/CPT-Soundings.pdf.
15. Song;, C. R.; Voyiadjis, G. Z. In *Pore pressure from penetrometer and hydraulic conductivity*, 15th International Conference on Soil Mechanics and Foundation Engineering Istanbul, International Society for Soil Mechanics and Geotechnical

Engineering: Istanbul, 2001; pp 279-282. https://www.issmge.org/uploads/publications/1/30/2001_01_0066.pdf.

16. Robertson, P. K., Soil behaviour type from the CPT: an update. 2010, https://www.cpt-robertson.com/PublicationsPDF/2-56%20RobSBT.pdf.
17. Robertson, P. K., Insitu testing and its application to foundation engineering. *Canadian Geotechnical Journal* 1986, *23* (4), 573-594.
18. Robertson, P. K., Soil classification using the cone penetration test. *Canadian Geotechnical Journal* 1990, *27* (1), 151-158.
19. Rockware, RockWorks17. https://www.rockware.com/product/rockworks/.
20. Putt;, A.; Kelly;, E.; Lowe;, K.; Rodriguez;, M.; Hazen, T., Effects of cone penetrometer testing on shallow hydrogeology at a contaminated site. 2021, http://hazenlab.utk.edu/files/pdf/2021Putt_EarthArXivcpt_effects.pdf.
21. K. Walker; E. Dixon; D. Joyner; K. Lowe; F. Poole; X. Ge; M. Thorgersen; D. Ning; Y. Fan; J. Michael; Y. Fu; R. Tian; Y. Wang; J. Van Nostrand; L. Lui; X. Wu; K. Davis; M. Adams; R. Chakraborty; D. Elias; R. Wilpiszeski; J. Zhou; M. Fields; T. Hazen; A. Arkin; Adams, P. In *ENIGMA Spatiotemporal Dynamics of Groundwater and Sediment: Geochemistry, Microbial Communities and Activities in Contaminated Aquifer*, Genomic Sciences Program Principal Investigator Meeting, 2020; https://enigma.lbl.gov/wp-content/uploads/2020/05/1_Walker_Hazen_ENIGMA_GSP_2020_Poster.pdf.
22. Hvorslev, M. J. *Time Lag and Soil Permeability in Ground-Water Observations*; Waterways Experiment Station: Vicksburg, Mississippi, 1951; p 53.
23. Puls, R. W.; Barcelona, M. J., Low-flow (minimal drawdown) ground-water sampling procedures. 1996, https://www.epa.gov/sites/default/files/2015-06/documents/lwflw2a.pdf.
24. Yeskis, D. a. Z., B. *Ground-water sampling guidelines for superfund and rcra project managers*; United States Environmental Protection Agency: 2002.
25. King, A. J.; Preheim, S. P.; Bailey, K. L.; Robeson, M. S.; Chowdhury, T. R.; Crable, B. R.; Hurt, R. A.; Mehlhorn, T.; Lowe, K. A.; Phelps, T. J.; Palumbo, A. V.; Brandt, C. C.; Brown, S. D.; Podar, M.; Zhang, P.; Lancaster, W. A.; Poole, F.; Watson, D. B.; Fields, M. W.; Chandonia, J. M.; Alm, E. J.; Zhou, J. Z.; Adams, M. W. W.; Hazen, T. C.; Arkin, A. P.; Elias, D. A., Temporal dynamics of in-field bioreactor populations reflect the groundwater system and respond predictably to perturbation. *Environmental Science & Technology* 2017, *51* (5), 2879-2889.
26. Dickson, A. G., An exact definition of total alkalinity and a procedure for the estimation of alkalinity and total inorganic carbon from titration data. *Deep-Sea Research Part a-Oceanographic Research Papers* 1981, *28* (6), 609-623.
27. H. Wickham, M. A., J. Bryan, W. Chang, L. D. McGowan, R. François, G. Grolemund, A. Hayes, L. Henry, J. Hester, M. Kuhn, T. L. Pedersen, E. Miller, S. M. Bache, K. Müller, J. Ooms, D. Robinson, D. P. Seidel, V. Spinu, K. Takahashi, D. Vaughan, C. Wilke, K. Woo, H. Yutani, Welcome to the tidyverse. *Journal of Open Source Software* 2019, *4*, 1686 https://www.tidyverse.org/.
28. Wickham, H., ggplot2: Elegant Graphics for Data Analysis. 2016, https://ggplot2.tidyverse.org.

29. Lasagna, M.; De Luca, D. A.; Franchino, E., The role of physical and biological processes in aquifers and their importance on groundwater vulnerability to nitrate pollution. *Environmental Earth Sciences* 2016, *75* (11).
30. Roberts, D., Soil properties, classification, and hydraulic conductivity testing. 1984, https://nepis.epa.gov/Exe/ZyNET.exe/.
31. Freeze, R. A.; Cherry, J. A., *Groundwater*. Prentice-Hall: Englewood Cliffs, N.J, 1979.
32. Asare, S. N.; Rudra, R. P.; Dickinson, W. T.; Wall, G. J., Seasonal variability of hydraulic conductivity. *Transactions of the ASAE* 1993, *36* (2), 451-457.
33. Moreels, D.; Crosson, G.; Garafola, C.; Monteleone, D.; Taghavi, S.; Fitts, J. P.; van der Lelie, D., Microbial community dynamics in uranium contaminated subsurface sediments under biostimulated conditions with high nitrate and nickel pressure. *Environmental Science and Pollution Research* 2008, *15* (6), 481-491.
34. Winston, R., *ModelMuse-A graphical user interface for MODFLOW-2005 and PHAST*. 2009.
35. Langevin, C.; Hughes, J. D.; Banta, E. R.; Niswonger, R.; Panday, S.; Provost, A., Documentation for the MODFLOW 6 Groundwater Flow Model. *Techniques and Methods* 2017.
36. Bailey, R. T.; Morway, E. D.; Niswonger, R. G.; Gates, T. K., Modeling variably saturated multispecies reactive groundwater solute transport with MODFLOW-UZF and RT3D. *Ground Water* 2013, *51* (5), 752-61 https://www.ncbi.nlm.nih.gov/pubmed/23131109.
37. Horton, N. J.; Kleinman, K., *Using R and RStudio for data management, statistical analysis, and graphics*. CRC Press: 2015.

Appendix A. Exploratory Nitrate Models

A.1 Methods

A 3-D visualization of the Area 3 was created using the ModelMuse v.4.3.0.0 (USGS) graphical user interface (GUI) with the MODFLOW 6 groundwater modeling software[4]. ModelMuse visualization uses stratigraphic data, which was based on the CPT results produced for this thesis and previous geology reports[2, 3]. The 3-D interpretation was the size and shape of Area 3, and the grid had 8 m squares and was enclosed in a larger grid so that the groundwater flow could be represented more accurately. The shallow subsurface stratigraphy was created by defining layers with differing hydraulic conductivities. The distribution of soil types and their corresponding hydraulic conductivities were measured by calculating the most frequently occurring soil types across three different depth ranges and regions within Area 3 using excel and RStudio. The regions were northwest, middle northwest, middle, middle southeast, and southeast. Each region contained about 6 CPT pushes. The three depth layers included the top layer, which was 0 to 3 m below ground surface, the middle layer, which was 3 to 6 m, and the bottom layer that was 6 to 9 m. The elevation of the terrain was added, as well[5]. Geometric objects were added to represent discontinuity layers, Bear Creek, and the wells that occupy the site. The discontinuity objects were given their own hydraulic conductivities and the Bear Creek object had its hydraulic head defined. The wells had their hydraulic heads and pumping conditions, if applicable. Inputs and parameters can be found in Tables A-1 through A-4.

One MODFLOW model was calibrated but not verified and labeled as exploratory. The flow model was meant to represent contaminant movement, and an initial contaminant concentration was used for the sink and source mixing package[5], which was volume of the S-3 ponds and several masses of nitrate over the years of operation of the ponds. A regression calculation was used to calculate the initial mass of nitrate at the starting time of operation. Nitrate was injected into the model through an object designated as the S-3 ponds using the Sink & Source Mixing package (SSM). MODFLOW 6 contains the Groundwater Flow model (GWF), in which a cell can be connected to other cells using hydraulic properties. Packages included in the GWF model can represent internal calculations of groundwater flow, like discretization and storage, stress scenarios, like wells and recharge, and advanced stress simulations like with unsaturated zone flow[4]. The program MT3D-USGS, a groundwater solute transport package,

Table A-1: The exploratory MODFLOW model parameters.

Model Parameters & Data Inputs	
Avg Kx	139 m/yr
Avg Ky	Avg Kx
Avg Kz	(Avg Kx)/10
Initial Head	Model Top - 3.5 m
Specific Storage	1.00E-05
Specific Yield	0.2
Model Top Elevation	2 m
Upper Aquifer Bottom Elevation	0 m
Middle Aquifer Bottom Elevation	-6 m
Lower Aquifer Bottom Elevation	-10 m
Longitudinal Dispersivity	10 m/yr
Porosity	0.25
Layers	3
Rows	31
Columns	42
Cells	3906

Table A-2: The time steps for the MODFLOW models (steady state was used for the calibrated model and transient for the exploratory model).

Time Inputs (years)					
Stress Periods	Starting time	Ending time	Length	Steady State/ Transient	Relative Years
1	0	10	10	Both	1951-1961
2	10	20	10	Both	1961-1971
3	20	30	10	Both	1971-1981
4	30	40	10	Both	1981-1991
5	40	50	10	Both	1991-2001
6	50	60	10	Both	2001-2011
7	60	70	10	Both	2011-2021
8	70	80	10	Both	2021-2031
9	80	90	10	Both	2031-2041
10	90	100	10	Both	2041-2051

Table A-3: The different packages and programs and their inputs for the MODFLOW models (the exploratory model didn't contain GHBEast2, GHBSouth, or GHBWest).

Packages and Programs Inputs		
Package Name	**Object Name**	**Values**
RIV: River	Area1BearCreek	Starting time: 0 yrs, Ending time: 100 yrs, River stage: Model_Top - 0.5 m, Conductance per unit length or area: 25 m/yr, River bottom: Model_Top - 1.5 m
DRN: Drain	DrainageCulvert	Starting time: 30 yrs, Ending time: 100 yrs, Elevation: Model_Top - 1.5 m, Conductance per unit length or area: 2E-5 m/yr
ETS: Evapotranspiration Segments	Evapotranspiration	Starting time: 0 yrs, Ending time: 100 yrs, Evapotranspiration rate: 0.65 m/yr, Evapotranspiration surface: Model_Top, Evapotranspiration depth: Model_Top - 1 m
GHB: General-Head Boundary	GHBNorth	Starting time: 0 yrs, Ending time: 100 yrs, Boundary head: 0.4 m, Conductance per unit length or area: 3.15E+9 m/yr, Z-coordinates: Upper to middle aquifers
GHB: General-Head Boundary	GHBEast	Starting time: 0 yrs, Ending time: 100 yrs, Boundary head: -1.06 m, Conductance per unit length or area: 3.15E+9 m/yr, Z-coordinates: Middle to lower aquifers
GHB: General-Head Boundary	GHBEast2	Starting time: 0 yrs, Ending time: 100 yrs, Boundary head: -4.44 m, Conductance per unit length or area: 3.15E+9 m/yr, Z-coordinates: Upper to middle aquifers
GHB: General-Head Boundary	GHBWest	Starting time: 0 yrs, Ending time: 100 yrs, Boundary head: -0.96 m, Conductance per unit length or area: 3.15E+9 m/yr, Z-coordinates: Middle to lower aquifers
GHB: General-Head Boundary	GHBSouth	Starting time: 0 yrs, Ending time: 100 yrs, Boundary head: -0.42 m, Conductance per unit length or area: 3.15E+9 m/yr, Z-coordinates: Middle to lower aquifers
RCH: Recharge & SSM: Sink and Source Mixing	S3WastePonds	Starting time: 0 yrs, Ending time: 30 yrs, Recharge rate: 0.35 m/yr & Starting time: 0 yrs, Ending time: 30 yrs, Nitrate concentration or mass-loading: 74,000 mg/L

Table A-4: Exploratory hydraulic conductivities and elevations for the MODFLOW models.

Object Inputs 1	
Object Name	**Value**
Area1Elevation	2.7 m
Area3Elevation	4.3 m
Area4Elevation	2.7 m
Elevation3_6	3.6 m
Elevation4_8	4.8 m
HillElevation	7 m
Mid32to37Bottom	81.68 m/yr
Mid32to37Middle	1.593 m/yr
Mid32to37Top	0.0173 m/yr
Mid38to43Bottom	835.7 m/yr
Mid38to43Middle	1.593 m/yr
Mid38to43Top	0.0173 m/yr
MidNW19to25Bottom	15,768 m/yr
MidNW19to25Middle	0.0173 m/yr
MidNW19to25Top	0.0173 m/yr
MidNW25ato31Bottom	61.81 m/yr
MidNW25ato31Middle	0.0173 m/yr
MidNW25ato31Top	0.0173 m/yr
MidSE45to48Bottom	20.81 m/yr
MidSE45to48Middle	1.593 m/yr
MidSE45to48Top	0.0173 m/yr
MidSE49to54Bottom	1.593 m/yr
MidSE49to54Middle	1.593 m/yr
MidSE49to54Top	0.0173 m/yr
MidSE55to57Bottom	0.0173 m/yr
MidSE55to57Middle	0.0173 m/yr
MidSE55to57Top	0.0173 m/yr

Object Inputs 2	
Object Name	**Value**
NW13to18Bottom	1.593 m/yr
NW13to18Middle	0.0173 m/yr
NW13to18Top	0.0173 m/yr
NW1to6Bottom	15,925 m/yr
NW1to6Middle	0.0173 m/yr
NW1to6Top	0.0173 m/yr
NW7to12Bottom	159.26 m/yr
NW7to12Middle	0.0173 m/yr
NW7to12Top	1.624 m/yr
ParkingLotElevation	5.4 m
RoadElevation	6 m
RoadElevation1Area1	1.5 m
RoadElevatiom2Area1	3 m
SE58to61Bottom	159.26 m/yr
SE58to61Middle	1.593 m/yr
SE58to61Top	0.0173 m/yr
SE61ato65	1.593 m/yr
SE61ato65Middle	1.593 m/yr
SE61ato65Top	0.0173 m/yr
SE66to70Bottom	1.593 m/yr
SE66to70Middle	0.0173 m/yr
SE66to70Top	0.0173 m/yr
SE71to73Middle	0.0173 m/yr
SE71to73Top	0.0173 m/yr
SE74to82Bottom	1.593 m/yr
SE74to82Middle	0.0173 m/yr
SE74to82Top	0.0173 m/yr
TankFarmElevation	3.7 m

Groundwater flow was calibrated with hydraulic head data and colloidal borescope measurements were calibrated with a bucket test calibration[1]. For this study, MODFLOW solved the groundwater flow equation using the finite difference approach (Equation 1), but can produce other outputs depending on the packages that are activated[6]. The most important inputs for simulating the groundwater and nitrate plume direction are the site elevations, initial hydraulic heads, and regions of recharge and discharge.

The nonparametric Wilcoxon signed rank test was used for not normally distributed paired data that contained pre- and post-treatment values to assess whether two samples were from the same population. The accepted significance level was set at 0.05[7]. Analysis of variance tests were used to determine if results were significant. The 2 factor ANOVA with replication was used for and within groups with two subgroups or elements. For instance, nitrate and hydraulic head groups each also had simulated and observed values. For the results to be significant, F values need to be larger than f critical and the p-value needed to be smaller than the alpha level set at 0.05.

$$\theta \frac{\partial C^k}{\partial t} + \rho_b \frac{\partial \overline{C}^k}{\partial t} = \frac{\partial}{\partial x_i}\left(\theta D_{ij} \frac{\partial C^k}{\partial x_j}\right) - \frac{\partial}{\partial x_i} \theta v_i C^k + q_s C_s^k - q_s^{'} C^k - \lambda_1 \theta C^k - \lambda_2 \rho_b \overline{C}^k$$

where

θ	is porosity or volume averaged water content (-),
C^k	is the dissolved concentration of species k, in units of mass per volume (M/L^3),
t	is time (T),
ρ_b	is the bulk density of the subsurface material (M/L^3),
$\overline{C}^k$	is the concentration of species k sorbed to the subsurface material, as mass/mass (M/M),
x_i and x_j	is the distance along the respective Cartesian coordinate axis, as length (L),
D_{ij}	is the dispersion coefficient tensor, as area/time (L^2/T),
v_i	is the linear pore water velocity (L/T),
q_s	is the volumetric flow rate per unit volume representing sources or sinks (T),
C_s^k	is the source or sink concentration of species k (M/L^3),
$q_s^{'}$	is the change in water storage per unit volume (1/T),
λ_1	is the first-order reaction rate for the dissolved phase (1/T),
λ_2	is the first-order reaction rate for the sorbed (solid) phase (1/T), and
∂	signifies the partial derivative of the variable that follows.

Equation 1: The equation solved by MT3D-USGS for the advection-dispersion-reaction of the groundwater flow system[4].

A.2 Results and Discussion

The MODFLOW model included some assumptions. If there were values, like dispersivity or conductance, that were not available via references or tests that could be done in the field, then the default values that ModelMuse provided were used. The exploratory MODFLOW and ModelMuse model of the nitrate plume shows the nitrate migrating in a south-southwest direction which supports previous studies[2, 3]. Flow boundaries were defined for each side of Area 3 so that groundwater was flowing through all of Area 3 despite there not being a well north of FW010. This is consistent with previous and current field studies of the groundwater flow direction. The exploratory model results are shown for present day (Figures A-1 through A-4) for the simulated nitrate concentrations and hydraulic head values was run without the inputs GHBEast2, GHBSouth, and GHBWest. The different colors represent the different concentrations of nitrate across Area 3. The models are shown at a depth range of 3.1 to 9.1 m BGS. The model simulated that well FW133-1 has the highest concentration at 24,904.79 mg/L and that well FW026 has the lowest concentration at 1,352.82 mg/L. For hydraulic head values, the model estimated that well FW133-1 has the largest hydraulic head value at -1.34 m and well FW026 has the smallest hydraulic head value at -2.11 m. The concentrations and hydraulic head values do not match what was seen in the field and need further analysis, but this was also a preliminary investigation of modeling the nitrate transport across Area 3. The MODFLOW simulation results were compared to the observed field results to see how closely the models mimic real-world processes for Area 3. The results were checked to see if they were normally distributed by plotting histograms. None of the data were normally distributed so the Wilcoxon test was run for each pair of nitrate concentration and hydraulic head observed and simulated results. Once the Wilcoxon test was run, then scatterplots were created to compare the results (Figures A-5 through A-8).

Tables A-6 and A-7 list the observed and simulated nitrate concentrations for each well in the exploratory and calibrated models. FW133-1, which had the highest observed nitrate concentration, also had the highest nitrate concentration in the MODFLOW model. The lowest observed nitrate concentration for FW134-2 did not match the simulated results, which indicated that FW026 had the lowest nitrate concentration and was orders of magnitude higher than the

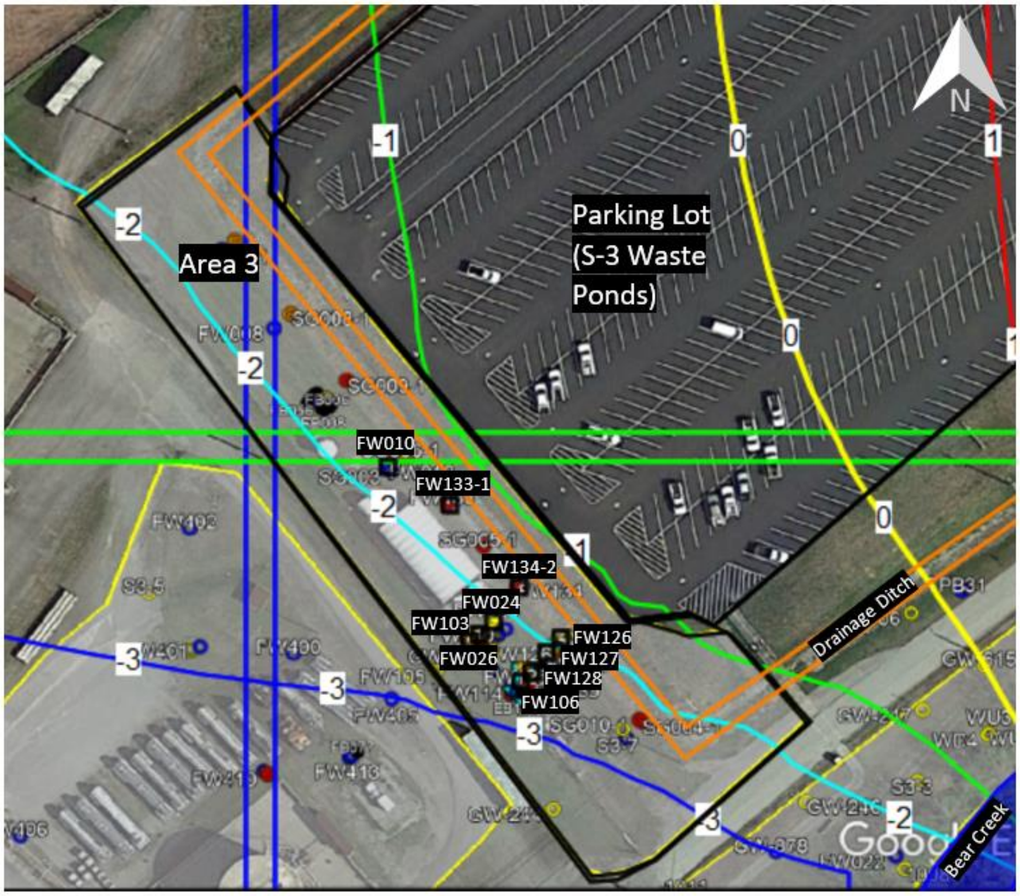

Figure A-1: The simulated hydraulic head contours for the transient exploratory MODFLOW model at a depth interval of 3.1 to 6.1 m BGS (wells FW010, FW133-1, and FW134-2). The blue, red, orange, and yellow circles represent different types of wells. 1,000 ft AMSL = 0 m AMSL (AMSL = above mean sea level).

(35° 58' 39.55"N, 84° 16' 25.37"W, eye alt 681 feet). Image taken from Google Earth, http://earth.google.com, Image Landsat/Copernicus (V 7.1., accessed November 6, 2021).

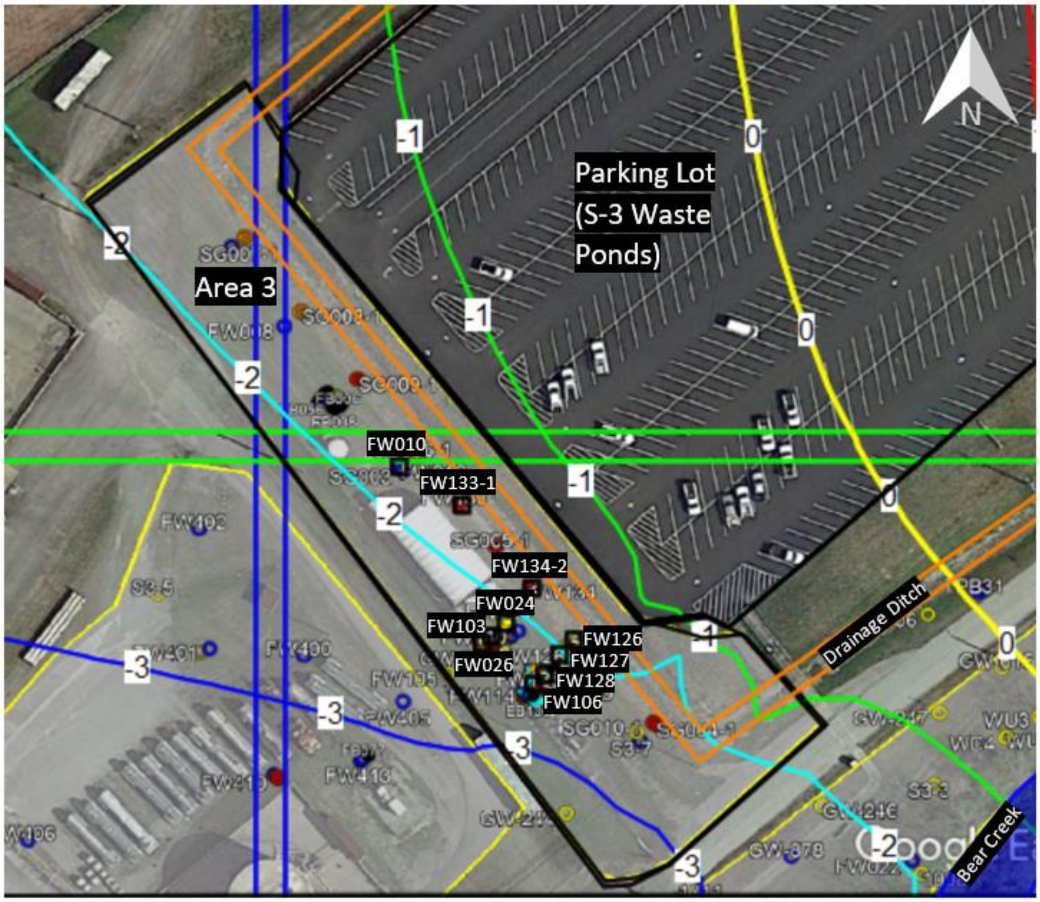

Figure A-2: The simulated hydraulic head contours for the transient exploratory MODFLOW model at a depth interval of 6.1 to 9.1 m BGS (wells FW024, FW103, FW026, FW126, FW127, FW128, and FW106). The blue, red, orange, and yellow circles represent different types of wells. 1,000 ft AMSL = 0 m AMSL (AMSL = above mean sea level).

(35° 58' 39.55"N, 84° 16' 25.37"W, eye alt 681 feet). Image taken from Google Earth, http://earth.google.com, Image Landsat/Copernicus (V 7.1., accessed November 6, 2021).

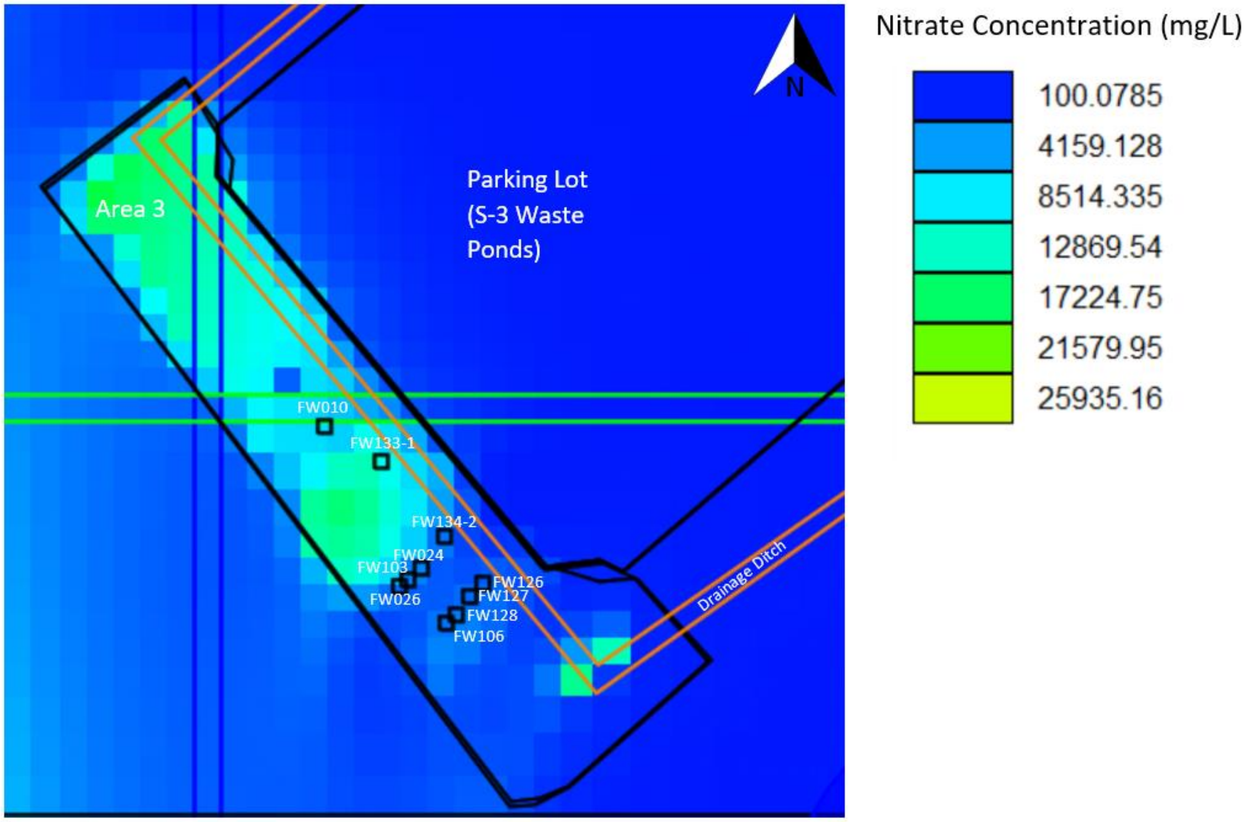

Figure A-3: The results of the simulated nitrate concentrations for the transient exploratory MODFLOW model at a depth interval of 3.1 to 6.1 m BGS (wells FW010, FW133-1, and FW134-2).

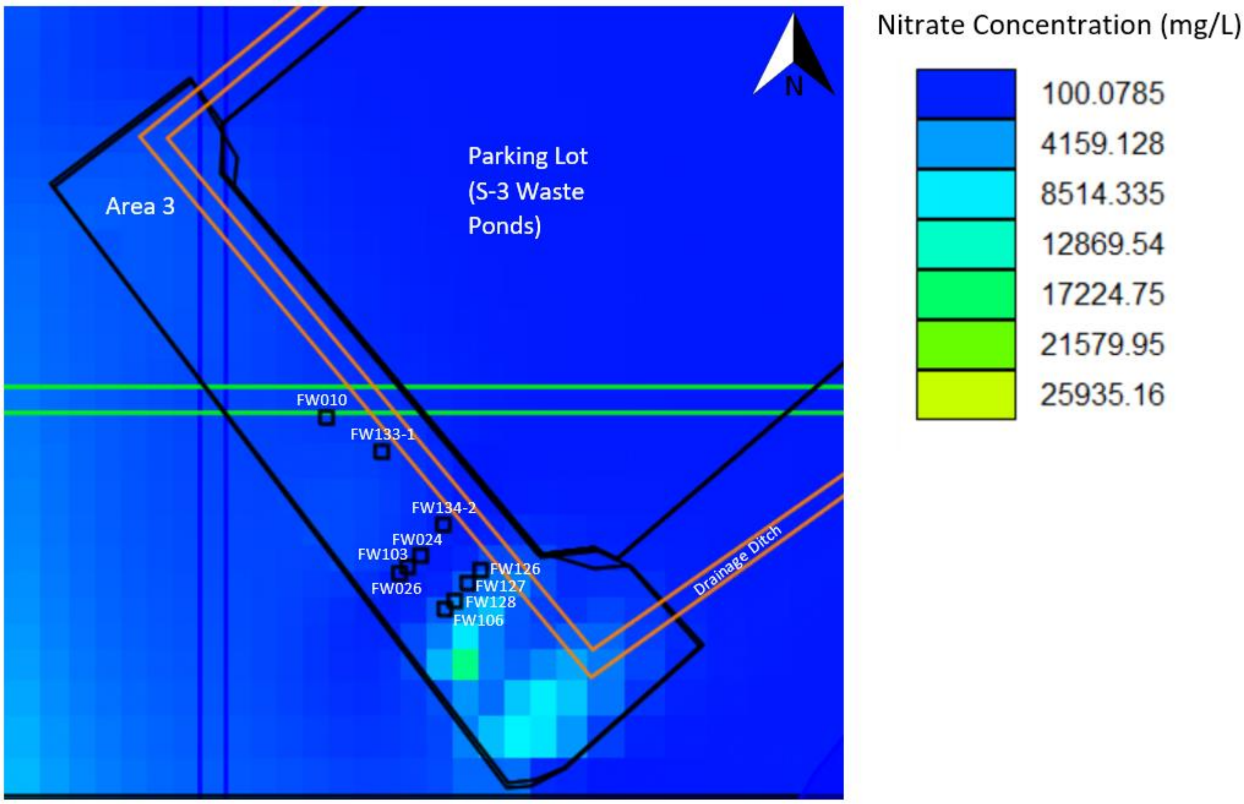

Figure A-4 The results of the simulated nitrate concentrations from the transient exploratory MODFLOW model at a depth interval of 6.1 to 9.1 m BGS (wells FW024, FW103, FW026, FW126, FW127, FW128, and FW106).

Table A-5: The observed hydraulic heads from the field and the simulated hydraulic heads from the calibrated steady state model.

Steady State Hydraulic Head Comparison		
Well	**Observed Head (m)**	**Simulated Head (m)**
FW126	-0.46	-1.1
FW133-1	0.55	-1.1
FW010	1.09	-0.83
FW106	-1.02	-0.89
FW128	0.18	-0.94
FW127	-0.44	-0.99
FW103	-0.55	-0.93
FW026	-0.45	-0.86
FW024	-0.44	-0.93
FW134-2	-0.06	-1.09

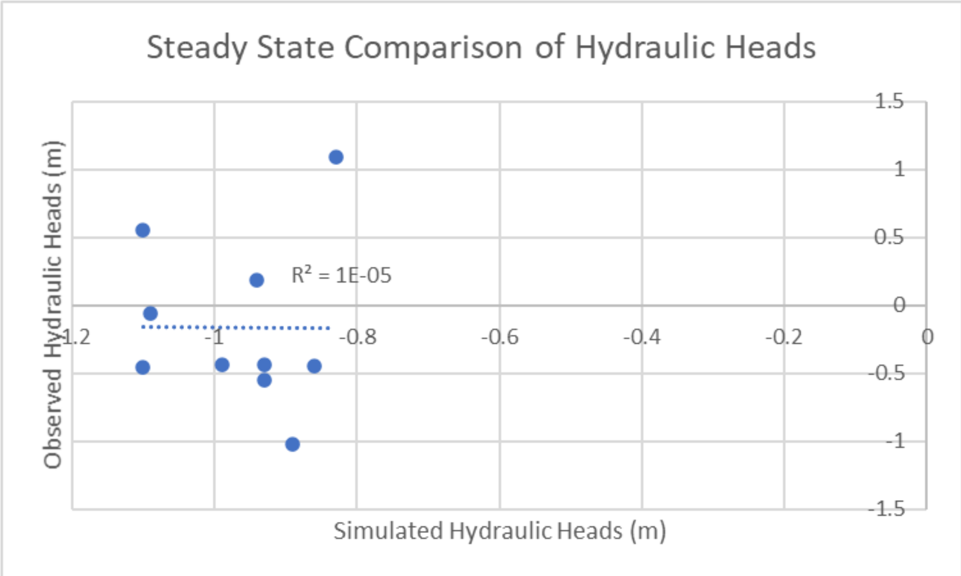

Figure A-5: A scatterplot comparing the observed hydraulic heads from the field and the simulated hydraulic heads from the calibrated steady state model.

Table A-6: The observed nitrate concentrations from the field and the simulated nitrate concentrations from the calibrated steady state model.

Steady State Nitrate Comparison		
Well	**Observed Nitrate (mg/L)**	**Simulated Nitrate (mg/L)**
FW126	7,098	713
FW133-1	36,676	11,169
FW010	19,794	5,709
FW106	1,829	1,170
FW128	5,083	3,017
FW127	2,989	1,152
FW103	985	140
FW026	0.29	140
FW024	5,870	140
FW134-2	0.22	2,055

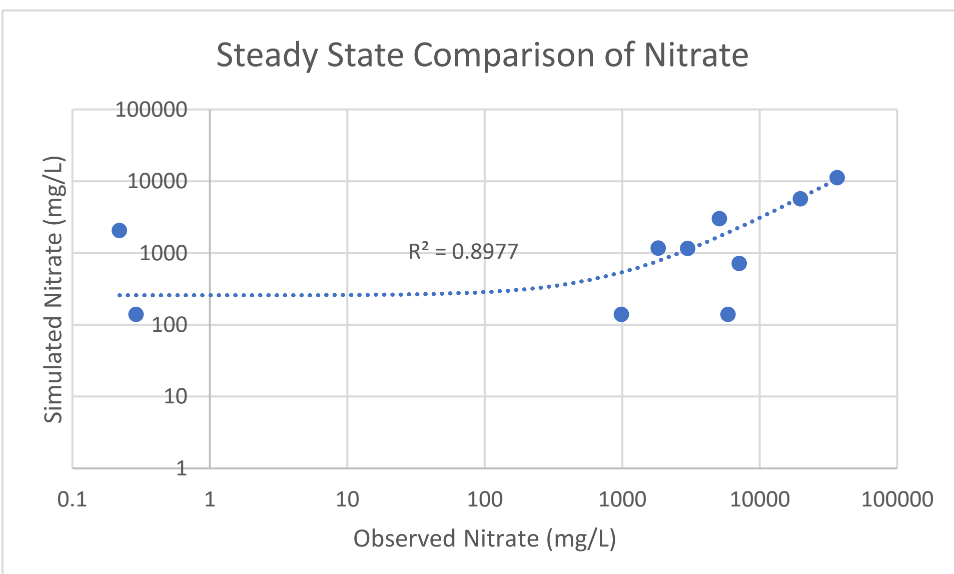

Figure A-6: A scatterplot comparing the observed nitrate concentrations from the field and the simulated nitrate concentrations from the calibrated steady state model.

Table A-7: The observed nitrate concentrations from the field and the simulated nitrated concentrations from the exploratory transient model.

Well	Observed Nitrate (mg/L)	Simulated Nitrate (mg/L)
FW126	7098.34	4771.22
FW133-1	36676.12	24904.79
FW010	19793.61	17784.37
FW106	1828.76	6396.15
FW128	5082.72	13481.43
FW127	2988.98	6459.12
FW103	984.82	1465.02
FW026	0.29	1352.82
FW024	5870.46	1465.02
FW134-2	0.22	5928.18

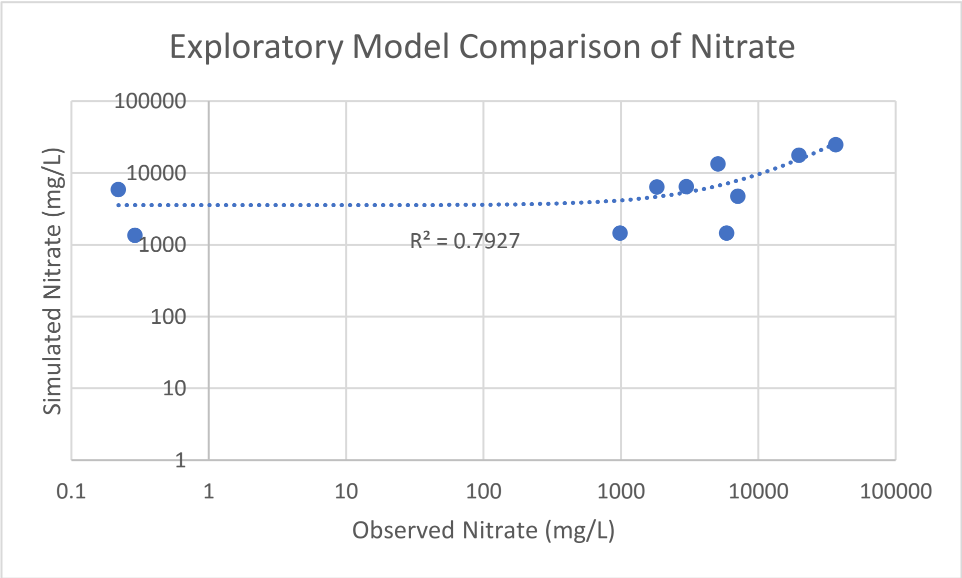

Figure A-7: A comparison of the simulated and observed concentrations for the nitrate plume seen in the field and exploratory transient model.

observed values. However, the Wilcoxon test comparing the observed nitrate plume to the field nitrate plume was significantly the same for both the steady state and transient models ($P=0.027$ and $P=0.0097$, respectively).

Tables A-5 and A-8 show the observed and simulated hydraulic head values for each well. The produced model values were based on water table measurements and site elevations. The shallowest observed hydraulic head values were wells FW010 at 1.09 m. The simulated hydraulic heads for this well were -0.83 and -1.42, respectively.

ANOVA with replication was run for the calibrated steady state model and the exploratory transient model. The different study variables that were analyzed (hydraulic heads and nitrate) are significant for both the exploratory and calibrated models ($P<0.05$). The value type (model simulated or observed in the field) was not significant for both the exploratory and calibrated models, as well as the interaction between study variables and value types because none of the p-values were significant. Because the study variables were significant, this suggested that a portion of the relationship between study variable (i.e., hydraulic head or nitrate) and corresponding value/concentration did not change based on the value type (i.e., simulated or observed). Also, the lack of significance for the interaction indicated that the relationship between a variable (i.e., hydraulic head or nitrate) and corresponding concentration/value does not depend on the value type, whether it be simulated from the model or observed in the field. Therefore, the value of the hydraulic head or nitrate concentration is independent of whether those values and concentrations are simulated from the model or observed in the field. This is the same result for both the calibrated model and exploratory model. Tables A-9 and A-10 summarize the results.

Table A-8: The observed hydraulic heads from the field and simulated hydraulic heads from the exploratory transient model.

Well	Observed Head (m)	Simulated Head (m)
FW126	-0.46	-1.56
FW133-1	0.55	-1.34
FW010	1.09	-1.42
FW106	-1.02	-2.03
FW128	0.18	-1.88
FW127	-0.44	-1.72
FW103	-0.55	-1.85
FW026	-0.45	-2.11
FW024	-0.44	-1.85
FW134-2	-0.06	-1.5

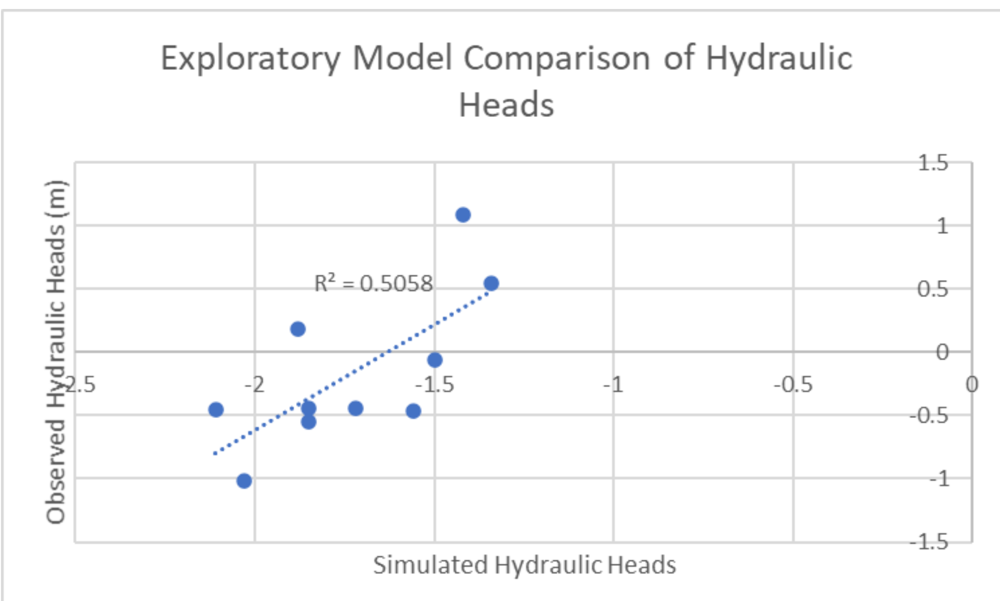

Figure A-8: A comparison of the simulated and observed hydraulic head values seen in the field and exploratory transient model.

Table A-9: Summary of ANOVA test run for the calibrated steady state models for the hydraulic heads and nitrate concentrations

Source of Variation	SS	df	MS	F	P-value	F crit
Nitrate/Hydraulic Heads (Rows)	279526756.5	1	279526756.5	7.59	0.01	4.11
Simulated/Observed (Columns)	75425426.84	1	75425426.84	2.05	0.16	4.11
Interaction	75381161.87	1	75381161.87	2.05	0.16	4.11
Within	1325042476	36	36806735.44			
Total	1755375821	39				

Table A-10: Summary of ANOVA test run for the exploratory transient models for the hydraulic heads and nitrate concentrations.

Source of Variation	SS	df	MS	F	P-value	F crit
Nitrate/Hydraulic Heads (Rows)	675283745.3	1	675283745.3	13.70	0.00	4.11
Simulated/Observed (Columns)	336381.28	1	336381.28	0.01	0.93	4.11
Interaction	342150.11	1	342150.11	0.01	0.93	4.11
Within	1774862577	36	49301738.25			
Total	2450824854	39				

Appendix References

1. McKay, L. D.; Sanford, W.; Strong, J. M., Field-scale migration of colloidal tracers in a fractured shale saprolite. *Ground Water* 2000, *38*, 139-147
2. Watson, D.; Kostka, J.; Fields, M.; Jardine, P. *The Oak Ridge Field Research Center conceptual model*; 2004, https://public.ornl.gov/orifc/FRC-conceptual-model.pdf.
3. Hatcher, R. D., Jr.; Lemiszki, P. J.; Foreman, J. L.; Dreier, R. B.; Ketelle, R. H.; Lee, R. R.; Lee, S. Y.; Lietzke, D. A.; McMaster, W. M. *Status report on the geology of the Oak Ridge Reservation*; United States, 1992; p 271, http://inis.iaea.org/search/search.aspx?orig_q=RN:24060945.
4. Winston, R., *ModelMuse-A graphical user interface for MODFLOW-2005 and PHAST*. 2009.
5. Langevin, C.; Hughes, J. D.; Banta, E. R.; Niswonger, R.; Panday, S.; Provost, A., Documentation for the MODFLOW 6 Groundwater Flow Model. *Techniques and Methods* 2017,
6. Bailey, R. T.; Morway, E. D.; Niswonger, R. G.; Gates, T. K., Modeling variably saturated multispecies reactive groundwater solute transport with MODFLOW-UZF and RT3D. *Ground Water* 2013, *51* (5), 752-61 https://www.ncbi.nlm.nih.gov/pubmed/23131109.
7. Horton, N. J.; Kleinman, K., *Using R and RStudio for data management, statistical analysis, and graphics*. CRC Press: 2015.

Vita

Erin Kelly graduated with a Bachelor of Science in Geosciences from Virginia Tech in May 2019. During her undergraduate career, she was a member of Geology Club and held the officer positions of museum representative and vice president. She also worked as an intern in the Museum of Geosciences at Virginia Tech and led the 2017 and 2018 GeoFairs which were hosted by the museum. She started graduate school at the University of Tennessee–Knoxville in August 2019 with Dr. Terry Hazen as her primary advisor. She completed the requirements for the Master of Science in Geology in the fall semester of 2021. She started a job as a staff hydrogeologist with Haley & Aldrich in August 2021.